COMPARATIVE STUDY OF EFFECTS TO RECORDING HEADS BETWEEN INTERNAL SHUNTING AND NON-INTERNAL SHUNTING

JIROPAST SUAKAEW

A THESIS SUBMITTED IN PARTIAL FULFILLMENT

OF THE REQUIREMENT FOR THE DEGREE OF

MASTER OF ENGINEERING IN DATA STORAGE TECHNOLOGY

ENGLISH PROGRAM

INTERNATIONAL COLLEGE

COLLEGE OF DATA STORAGE TECHNOLOGY AND INNOVATIONS

KING MONGKUT'S INSTITUTE OF TECHNOLOGY LADKRABANG

2011

KMITL-2011-IC-M-005-002

Thesis	Comparative Study of Effects to Recording Heads between Internal Shunting and Non Internal Shunting
Student	Mr. Jiropast Suakaew
Student ID.	52600615
Degree	Master of Engineering
Program	Data Storage Technology
Year	2010
Thesis Advisor	Dr. Kasin Vichienchom. (Advisor)
	Assoc. Prof. Dr. Wanchai Pijitrojana. (Co- Advisor)

ABSTRACT

This research is comparative study of effects to recording heads between Internal Shunting (IS) and Non Internal shunting. IS has been introduced on the tunneling magneto resistive heads to enhance the device anti-static robustness and the external high-frequency noise pickup immunity. The shunting scheme and its mechanism lead to both increasing anti-static robustness and reducing high-frequency noise pickup. To analyse the effects of IS vs non-IS, the readout signal amplitude and the head resistance are used as the key parameters to measure the outcome by comparing the head performance of IS and non-IS at the beginning of the assembly process with that at the ending of the assembly process. The study results show failure of IS and non-IS while processing through production are not significantly different from sample recording head that being tested. The robustness of recording head is then verified using life test. The 7,000 Hrs life tests with multiple stress levels sets varied from low to high voltage are applied to recording heads. The readers are intentionally damaged until resistance changed to target value. There is no sign of difference of resistance and amplitude changed with time and voltage from two groups of samples, IS and non-IS.

Acknowledgements

I would like to thank Associate Professor Dr. Wanchai Pijitrojana and Dr. Kasin Vichienchom, my advisors, for their helpful suggestions and supports during this research at KMITL. I am also thankful to all thesis committee members for their constructive comments and helpful discussions, which gave me a better perspective on my own results. I should also mention that my graduate study at King Mongkut's Institute of Technology Ladkrabang was financially supported by NSTDA, KMITL and Seagate Technology (Thailand) Ltd.

Thanks are also to my beloved father, mother, wife and my kids who triggered & supported me to do this Master Degree in Data Storage Technology.

JIROPAST SUAKAEW

Contents

Page

Contents (Cont.)

Page

Contents (Cont.)

Page

List of Figures

Figure **Page**

List of Figures (Cont.)

Figure Page

List of Figures (Cont.)

Figure **Page**

List of Tables

Table **Page**

CHAPTER 1

Introduction

1.1 Problem statement

The use of an ultra-thin insulating barrier and the presence of conductive paths in the form of pinholes are the key concerning for the performance of the tunneling magneto resistive (TMR) sensor to be indeed easily degraded by ESD [4-7]. To handle this matter, the internal shunting (IS) has been introduced on (TMR) head [2]. It is able to enhance anti-static robustness and external high-frequency noise pickup immunity of the device. Details of simplified schematic diagram of the recording head with and without shunting are shown in Fig. 1.1 (a) and (b).

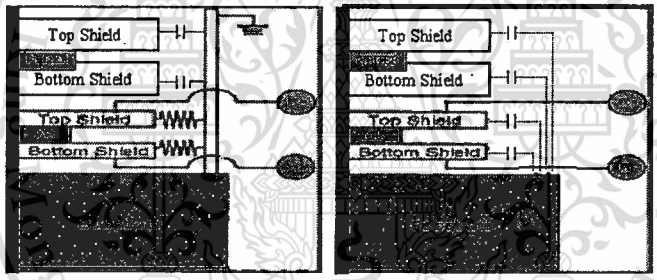

Figure 1.1 Schematic diagram of recording head (a) IS and (b) Non-IS

For the recording head with IS as shown in Fig.1.1 (a) If capacitance between writer bottom shield-to-top MR shield and substrate-to-bottom MR shield are balanced, noise injection on both top and bottom shields will be the same for both amplitude and phase. Therefore, noise will be cancelled out for the differential read back signal. In case of non-IS as shown in Fig.1.1 if noise frequency is high enough, noise current from the substrate can be injected into TMR sensor due to unbalanced coupling to the top and bottom shields. Since the top and bottom shields constitute the two leads of the TMR device, this high-frequency noise signal will affect the spectral signal-to-noise ratio measurement.

1.2 Objective

To analyze the effect of IS vs non IS, the readout signal amplitude and the head resistance are used as the key parameters to measure the outcome by comparing the head performance of IS and non IS at the beginning of the assembly process with that at the ending of the assembly process. Some noise and instability parameters such as asymmetry are included in the analysis as well. The robustness of recording head is then verified using life test.

1.3 Research Benefit

1.3.1 To understand physic of reader structure and circuit.

1.3.2 To understand the recording head performance of IS vs Non IS.

1.3.3 To obtain the robustness of the non IS head.

1.3.4 To develop for new HD structures align with current production environment.

1.4 Research Methodology

1.4.1 Using the readout signal amplitude and the head resistance by comparing the head performance at the beginning of the assembly and the ending of the assembly process.

1.4.2 Study the head characteristics with static electrical test.

1.4.3 Study the robustness of recording head with life test.

1.4.4 Analysis the head performance by varying voltage applies to blow IS.

1.5 Scope of Research

1.5.1. Using the current head as the experiment.

1.5.2. Compare read back from IS and non IS of each difference blow time (short, medium and long time).

1.5.3. Life test will use the real test at 400hrs and then use statistical method for performance prediction.

1.6 Thesis Organization

This thesis is organized in the following way manner. Chapter 2 presents the literature review and principle of HD operation; Chapter 3 presents the fundamental concepts of ESD; Chapter 4 presents design of experiment; Chapter 5 presents results and conclusions. This research work will be concluded and some importance issues for future work will be also given. Appendix A represents the failure model testing.

CHAPTER 2

Literature Review and Fundamental of Recording Head

2.0 Literature Review

There are total of 4 papers reviewed for this study to understand the topic. The papers are organized as

1. The load resistance limitation [1]
2. Shunt tab process to GMR [2]
3. ESD behavior on Disk Drive [3]
4. Anti-Static Robustness Enhancement with Internal shunt [4]

The work in [1] helps us to understand the load resistance of the MM and HBM tester It can significantly influence the peak value and shape of the discharge transient current during ESD testing. For devices that have an energy (current) failure mechanism, e.g. GMR and TMR heads, reporting a failure voltage alone can lead to misleading interpretation of ESD sensitivity. It is concluded that the comparison of ESD robustness should be based on the actual current or energy, not the charging voltage value alone.

In [2], it describes the trim shunt tab process may cause the damage of GMR heads due to the raised voltage between the GMR sensor lead and the bottom shield. This may also possibly destroy the GMR sensor at the beginning of trimming process. It is also seen that the time interval of trimming may affect a GMR head as the longer cutting time the higher raised voltage between the GMR leads and the bottom shield. The trimming time interval between each leads of an order of 300 ps or longer may cause the raised voltage above 30 V between the GMR leads and the bottom shield.

In [3], it describes the behavior of a disk drive during an ESD event can be understood in terms of the voltage time constant for each component, as well as the relative strength of the coupling between each component. Due to different time constants and coupling between each component in a drive, the voltage on the base, disk, slider and GMR sensor can lead or lag each other during grounding of the disk. The worst case is when there is a large range in time constants for the internal components, weak coupling between components, and low resistance grounding of the disk. This situation results in the equivalent of "The Perfect Storm" and results in the largest possible voltage differences between internal components. When the voltage difference between the slider or GMR sensor exceeds the breakdown voltage to the disk, which in some cases is only 3V, electrical breakdown can damage the disk and GMR sensor. This breakdown was observed experimentally using a hybrid drive. While in general the disk drive is extremely robust against ESD damage, electrical breakdown between internal components in extreme cases of poor drive design and handling are combined. It is concluded that it is extremely important to understand the behavior of the voltage on the internal components inside a disk drive when a charged drive is grounded.

In [4], Internal shunting can enhance the anti-static robustness of the entire product. This is because static charge can no longer accumulate around the TMR sensor and any discharge current will not be high enough to damage the TMR sensor. Furthermore, internal shunting can achieve external noise current compensation by shorting the writer shield and balancing the capacitance between the top shield and the writer shield and the one between the bottom shield and the substrate. Grounded substrate with small impedance is also effective for minimizing the noise on the TMR sensor by shunting the external noise current directly to the suspension ground.

2.1 Writing in Perpendicular recording

The perpendicular recording technology, it is used in HDD for a few year ago to support high-density magnetic data storage, since it is technically the closest to conventional longitudinal compared with other technologies and methods. The

significant difference between perpendicular and longitudinal recording is that the former orients the magnetization of the recording bit normal to the surface of the medium, thereby saving space in the plane of the medium and increasing thermal stability. The typical perpendicular recording model is shown in Fig. 2.1. There are three key elements in perpendicular recording: a single pole perpendicular writes head, an anisotropy recording film and a soft magnetic underlayer (SUL).

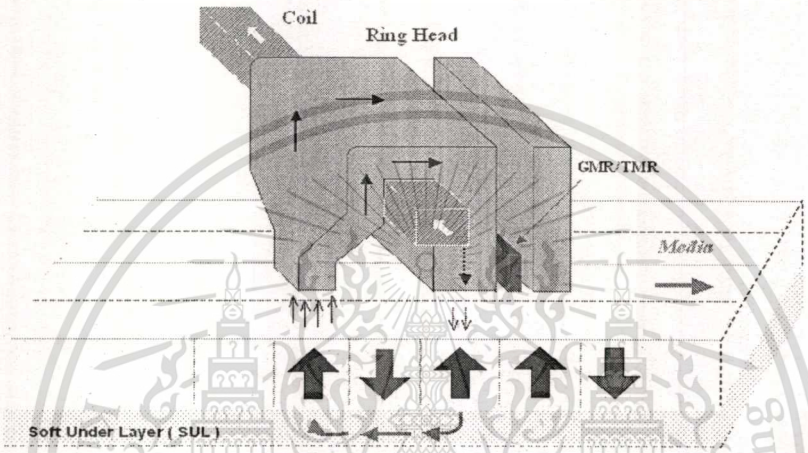

Figure 2.1 A typical perpendicular recording model: a magnetic recording medium and a soft under layer (SUL) used together with a single-pole head [Seagate]

2.1.1 Single pole write head (SPH)

In conventional longitudinal recording, the maximum field generated from a ring head (RH) is limited by 2¶*Ms*, where *Ms* is the saturation magnetization of the write-pole material while in perpendicular recording the write field is generated between the trail pole of a single pole head and a soft underlayer. In this geometry, the upper limit of the write field is 4¶*Ms*, twice the field from the longitudinal recording head. The ability to generate higher fields makes it feasible to record bits on a higher magnetic anisotropy medium, which in turn further delays the superparamagnetic limit to a higher areal density. [8] Thereby, to realize higher-resolution writing, a strong and sharp perpendicular field from a single pole type writes head is required. [9–11] This requires that a single pole write head should be designed to energize the recording medium. A recording layer should consist of a single pole head and a double-layered medium. Also, a soft magnetic back layer is designed to effectively

bring out the effect of magneto static interaction between them. Besides, the recording layer of the medium should be made to narrow the dispersion of the grain size and coercivity.

A detailed overview of the methodology to design a write transducer for recording onto perpendicular media at areal densities beyond 1Tbit/in^2 is presented. The two basic modes of perpendicular recording, single-layer recording media in combination with a ring type head and double-layer recording media with a soft underlayer in combination with a single pole head, are compared with each other theoretically and experimentally. In addition, perpendicular recording is compared to longitudinal recording from the perspective of the writing process. The system efficiency is redefined for perpendicular recording to take into account the critical role of the soft underlayer. The effects of using "soft" magnetic shields around the trailing pole are analyzed. It is shown that at least a factor of two increases in the field can be obtained at areal densities beyond 500 Gbit/in^2 if shields are used. Such an open issue as the skew angle sensitivity in perpendicular recording is analyzed. It is shown that using "soft" magnetic shields around the trailing pole substantially improves the skew angle sensitivity. Moreover, using shields substantially improves the system efficiency and to some degree fulfils the role of the soft underlayer in perpendicular recording.

The magnetic recording process utilizes a thin film transducer for the creation or writing of magnetized regions (bits) onto a thin film disk and for the detection or reading of the presence of transitions between the written bits. The thin film transducer is referred to as a thin film head. It consists of a read element, which detects the magnetic bits and a write element, which creates or erases the bits. Fig. 2.2 shows a perspective view of the thin film head as viewed from the surface of the disk. In a disk recording system, successive bits are written onto the disk surface in concentric rings or tracks separated by a guard band. The head transducer is attached to a suspension, and the suspension is attached to an actuator, which controls the position.

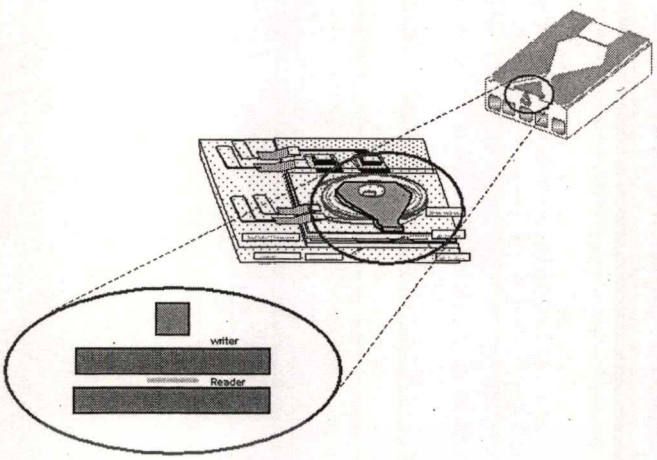

Figure 2.2 Thin-film head structure as viewed from the media disk surface [Seagate]

A more detailed description of the Single Pole Head (SPH) structure is presented with the purpose to explain the approach chosen to design the SPH geometry, as shown in Figure 2.3, and thus clarify the limitations of this head design and motivate an approach for future modifications. The limitations are fundamentally caused by the inability to infinitely maintain the linear scaling of the system dimensions (for increasing the areal density) below the value, at which the flying height reaches its smallest value that is physically feasible. It is believed that it is unlikely to be able to maintain a steady flying height below approximately 5 nm because of the proximity to the size of the air molecules critically participating in the recording head flying process. Therefore, a deviation from the straightforward scaling law is necessary for further increasing the areal density.

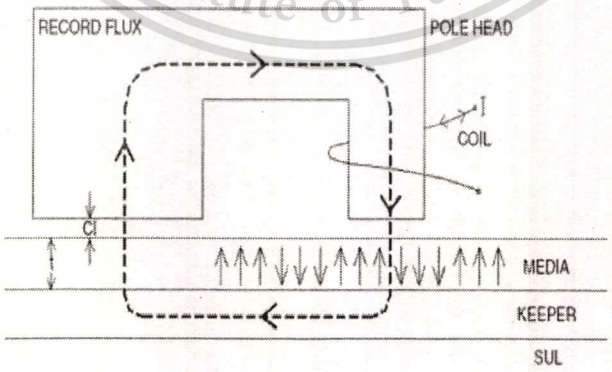

Figure 2.3 A schematic diagram of a Single Pole Head (SPH) [46]

This deviation can be accomplished through the modification of the SPH design. Hence, the understanding of the principles utilized to design SPH geometry shall make SPH modifications most efficient for satisfying the demand for the areal density increase. Before going into details, it is worth reminding the major requirements towards a write head in perpendicular recording:

1) The ability to generate a sufficiently strong field for recording onto a medium with adequate coercivity.
2) The ability to localize the recording field in a fairly limited region along the track so that the skew angle sensitivity is minimized.
3) The ability to maintain reasonable efficiency of a recording system.

Before going into a description of the design methodology, it is worth reminding that already today the flying height in every state-of-the-art recording system is of the order of 5 nm, which is already close to the size of the air molecule. Therefore, it is hard to see how the flying height can be further reduced, because the air flow process is a critical link in the ultimate operation of a magnetic hard-drive. This means that the established over decades trend of increasing the recording density in a magnetic recording system only through the direct application of the scaling law should be adjusted for creating next generation magnetic technologies. In other words, for obtaining the maximum benefit and achieving the highest possible areal density, special attention should be given to each component of the magnetic recording system.

2.1.2 Throat Height Dependence

The throat, being the narrowest part of the magnetic flux loop (circuit), typically, is also the highest reluctance link of the magnetic loop [12]. Thus, by reducing the throat height, the relative contribution of the throat region into the net reluctance of the magnetic circuit is also reduced and therefore, the overall efficiency of the system is increased. Also, by reducing the throat height, the recording field at saturation is increased. There are two competing factors contributing into the

increase of the recording field as a result of the throat height reduction. First, the field is increased because as a result of the throat height reduction the point inside the pole tip at which the saturation starts to occur is shifted closer to the ABS. Calculated magnetization contours along the central cross-track planes inside the main pole tip in two extreme cases, with fairly tall and sufficiently short throats, are shown in Figures 2.4a and b, respectively. The magnetization profiles at saturation along the central vertical line inside the pole tip for these two cases are shown in Figures 2.4c. It can be observed that for the tall throat, the saturation occurs near the top region of the throat, thus only a relatively small part of the initial magnetic flux generated by the drive coil reaches the ABS. As the current is increased beyond the saturation value, the most of the flux is going to leak out from the magnetic loop on its way from the drive coil to the ABS. In contrast, for the short throat, the saturation starts to take place at the ABS, thus the maximum possible flux reaches the ABS and therefore the maximum possible field (for a flat surface, of the order of 4¶*Ms*) can be generated. In other words, in the latter case, there is effectively more magnetic "charge" generated at the ABS. The "charge" at the ABS is the required source of the recording field.

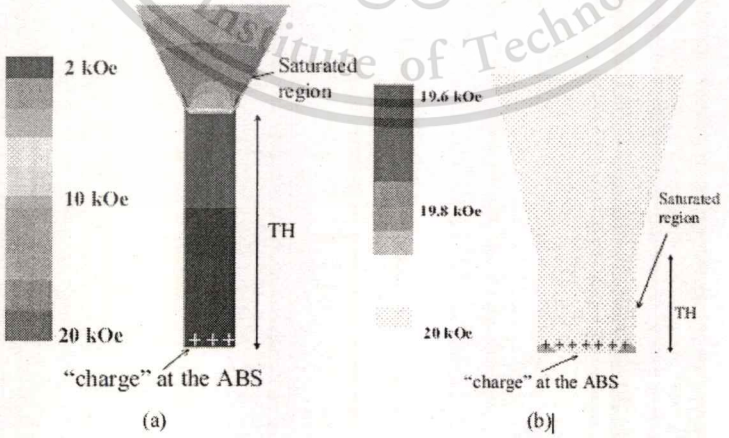

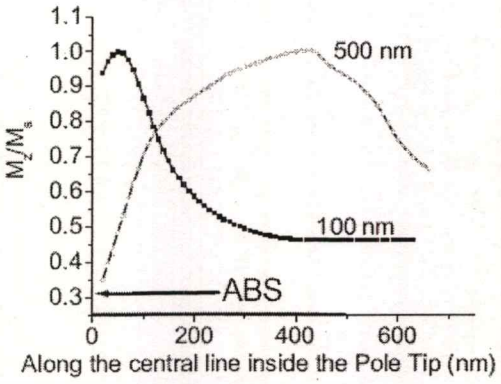

(c)

Figure 2.4 Calculated magnetization contours along the central cross-track planes inside the main pole for two extreme cases at saturation (a) a fairly tall throat and (b) a sufficiently short throat. (c) Magnetization profiles along the central vertical line for the two cases at saturation [48]

Because the charge is located at the ABS, the pole tip determines the recorded bit sizes. Therefore, being local by its origin, this is a favorable effect of the throat height reduction. Unfortunately, the throat height reduction results in another effect, which deteriorates the field gradients. This effect is due to the "charges" created on the tilted walls above the throat height of the main pole, as shown in Figure 2.4. These "charges" generate an extra field, which is not localized and therefore results in the deterioration of the field gradients. As the throat height is reduced, the "charge" at tilted walls is effectively moved closer to the ABS, and thus, the effective contribution of this unfavorable field increases. It should be remembered that although a perpendicular medium is ideally symmetric with respect to any of the two in-plane directions. Because of fabrication process limitations, typically, the throat top boundaries (the line at which walls starts to deviate from being vertical) are defined only at the two cross-track side walls of the main pole, and not at any of the two along-track side walls, as shown in Figure 2.5. It should be reminded that the magnetic "charge" is proportional to the change of the magnetization component normal to the boundary surface [13]. Therefore, in the particular case, the magnetic "charge" is concentrated on the cross-track sides rather than on the leading and trailing sides of the main pole. As a result, because of the different amount of the

"charge" in these two cases, the throat height dependencies might be quantitatively different for the field profiles along and across the track, respectively, as shown below.

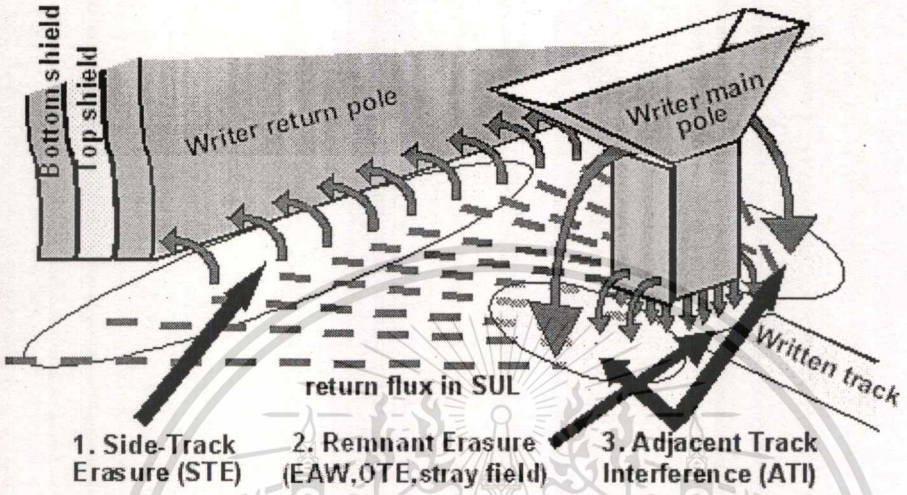

Figure 2.5 A diagram of a SPH pole tip showing location of side wall "charge" [Seagate]

2.1.3 Multiple Magnetic Image Reflection

In a perpendicular system recording is produced by the trailing edge of the trailing pole (TP) of a single pole head (SPH), as shown in Figure 2.6. The electrical current in a coil wrapped around the TP controls the recording field. However, additional field sources contribute to the net recording field under the TP. Previously, it was shown that the additional sources are due to the magnetic "charge" in a recording medium, which, unlike in longitudinal recording, is concentrated not in the transitions, but rather more uniformly distributed at the top and effective (due to the presence of the SUL) bottom sides of the recording layer. Among these sources is the field generated by tracks adjacent to the main track under the TP. From the field superposition principle, the maximum field in this case is less than 2¶*Ms*, where Ms is the saturation moment of the recording layer. This effect exists in both longitudinal and perpendicular recording leading to non-linear transition shift (NLTS).

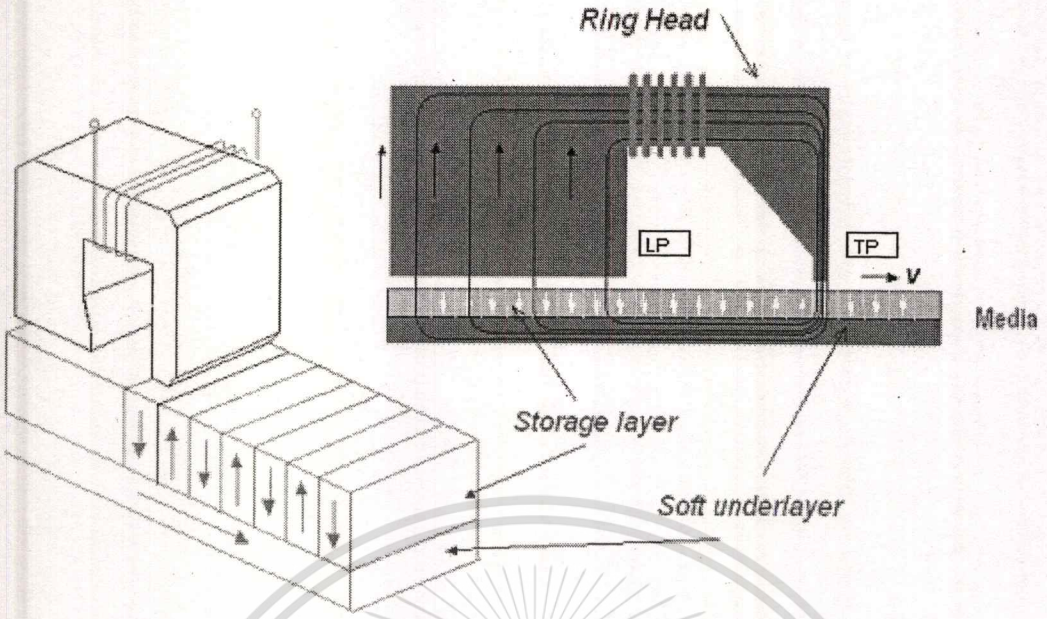

Figure 2.6 A schematic diagram showing how due to the multiple reflection a relatively small field under the leading pole can be magnified into a relatively strong field under the trailing pole [Seagate]

There is an additional effect inherent only to perpendicular recording with a SUL, which contributes to the net field under the TP. The magnetic flux due to a bit-pattern in the recording layer can be transferred from the leading pole to the trailing pole, as shown in Figure 2.7. Although indirect, this effect is capable of generating a relatively large additional field under the TP, as shown below. As described below, the process underlying this effect can be explained in terms of the multiple (magnetic) image reflection (MIR) of the surface magnetic charges in the recording layer, sandwiched between two magnetic "mirrors", the soft underlayer and the leading pole.

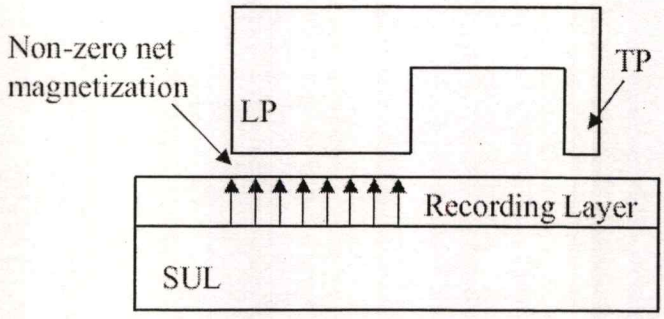

Figure 2.7 A schematic diagram showing the origin of the MIR effect [46]

The intention of this section is to utilize 3-D boundary element modeling (BEM) supported by spin-stand and magnetic force microscopy (MFM) experiments to investigate in detail the dependence of various parameters on the MIR effect. In the absence of two magnetic mirrors above and below the recording layer, the stray field emanating from a DC magnetized recording layer is negligibly small. The net stray field is a sum of the oppositely directed fields generated by the top and bottom surface "charge" of the recording layer. In other words, the magnetic field is "trapped" inside the recording layer, as shown in Figure 2.8. Next, the effect of the presence of the soft underlayer and the leading pole can be analyzed. As earlier described, the soft underlayer acts as a mirror that creates an image of the surface charge in the recording and thus increases the effective separation between the effective bottom and top charge in the recording layer. The leading pole is the second magnetic mirror added to the opposite side of the recording layer. This second mirror creates another set of surface charge images and further increases the effective separation between the effective bottom and top charge. The following analogy could illustrate the rest in this process. Imagine yourself standing between two facing each other mirrors. Ideally, due to the multiplicative reflection you should be able to see an infinite number of images of yourself. Similarly, this multiplicative process leads to the effective substantial separation of the surface charges from each other and thus, releases non-zero magnetic flux Ideally, assuming the head/medium system to be a 100% efficient magnetic flux guide, i.e., with no flux leakage, according to the magnetic flux conservation, assuming a Demagnetized medium under the leading pole, the magnitude of the additional field, $H_{addition}$, generated under the trailing pole is expected to be directly proportional to the net magnetic

moment of the recording layer, Ms, $H_{addition} = 4\P M_s A_{LP} / A_{TP}$, where A_{LP} and A_{TP} are the ABS areas of the leading and trailing poles, respectively. The linear dependence on the Ms and the ratio A_{LP}/ A_{TP} is valid as long as no saturation occurs in the system. The linear dependence on the ratio A_{LP}/ A_{TP} becomes a crude approximation when the track width and, consequently, the area, A_{TP}, is reduced down to a size, at which the efficiency of the system starts to drop. Previous calculations indicate that for a given perpendicular system configuration the efficiency drops to values less than 60 percent as the track width becomes narrower than approximately 300 nm. At such narrow track widths, significant amount of the magnetic flux generated in the region under the leading pole due to the MIR effect leaks out on its way to the trailing pole.

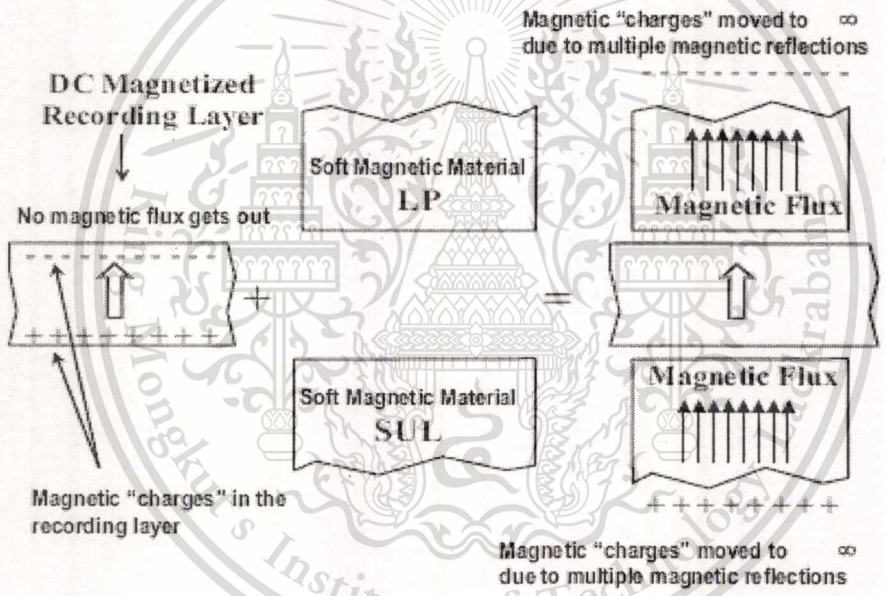

Figure 2.8 A schematic diagram helping understand the difference between two cases: a) magnetic flux trapped inside the recording layer and b) the magnetic flux extracted from the recording layer region located between SUL and LP due to the MIR effect [48]

2.1.4 Shielded Single Pole Head

One of the previously proposed solutions is to build "soft" magnetic shields around the main pole, as shown in Figure 2.9.

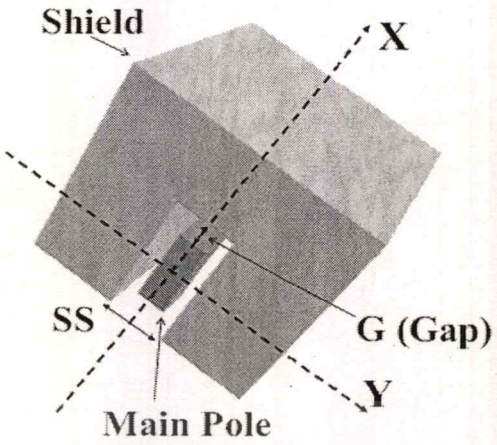

Figure 2.9 A diagram of the ABS view of a shielded single pole head (SSPH) pole tip configuration [48]

It can be noted that the shields are wrapped only around the trailing side and the two cross-track sides of the main pole. Only these three sides are critical for recording, because the two cross-track sides define the track width and the trailing side defines the quality of each linear transition. No recording is supposed to take place at the leading side; therefore, this side does not necessarily have to be covered with a shield. The direct effect of the shielding is screening the unfavorable side field away from the recording medium, as shown in a cross track cross-section diagram in Figure 2.10. Consequently, the constraints on the head structure, which were put on the regular SPH (without shielding) for the purpose of reducing the effect of the side field, are substantially relaxed if shields are utilized. It should be reminded that for the regular SPH, the pole tip geometry is chosen with a fairly large throat height with the purpose to reduce the side field. The cost of the fairly tall throat is the substantial reduction of the field magnitude and the system efficiency, as shown above. On the contrary, for the case with shields, the throat height can be substantially reduced for maintaining the fairly large field magnitude without loosing the field gradients. In other words, if shields are used, a substantially more efficient pole structure can be implemented without loosing the field gradient. Possible today throat height is going to be dictated by the lapping process accuracy. As a direct consequence of the ability to exploit a more efficient pole tip configuration, the improved skew angle performance of SSPH can be mentioned. Due to the higher efficiency, as compared to SPH, a much thinner pole tip can be utilized to generate

the same recording field. Therefore, SSPH has substantially improved skew angle performance, as compared to that of SPH.

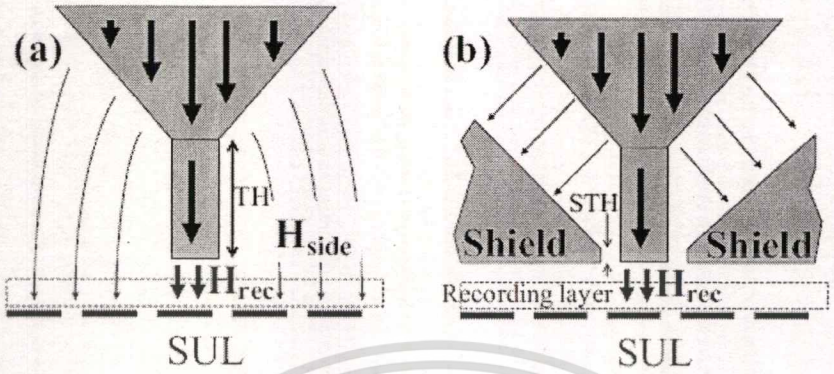

Figure 2.10 Diagrams showing the magnetic field propagation for the two cases of interest: (a) without and (b) with shields [48]

For the SSPH design, the side cross-track and trailing field gradients are dominantly determined by the spacing between the main pole and the shields. This is in contrast with the regular not-shielded SPH design, for which the gradients are determined not only by the flying height and the separation between the ABS and the SUL but also to significant degree by the throat height. Evidently, the deadly limitation of a nonzero throat height in the case of the regular SPH design is automatically removed in the case of the SSPH design. In the latter case, even for a substantially shorter throat height, the undesired side cross-track and trailing fields are reduced due to the existence of a relatively low reluctance and well-defined return flux path via the shields. As noted above, the reduction of the throat height to zero drastically increases the system efficiency and allows a substantially larger amount of the magnetic flux generated by the drive coil to reach the ABS. This automatically results in an improved skew angle performance of the SSPH design, as compared to the conventional SPH design, because in this case a head with a substantially thinner pole tip can be utilized to generate a field as strong as the field generated by an equivalent conventional SPH with a much thicker main pole tip. The skew angle sensitivity is proportional to the pole tip thickness. Another observation that can be made is the fact that if shields around the main pole are utilized, as described above, there is absolutely no need for the return pole separated with a fairly large

gap from the leading edge of the main pole, as shown in Figure 2.11a. The shields wrapped around the main pole not only act as the gradient shapers but also perform the role of a return pole. As a result, a system with shields around the main pole and without a return pole remains approximately as efficient as a regular system with a return pole. As a consequence of the shields acting also as a flux return pole, the requirements on the use of a SUL are much less tight as compared to the regular SPH case. It can be also observed that the shielded structure resembles the typical ring head structure. The purpose of the separation between shields and the main pole is to avoid the side field and thus to distinctly define the recording transitions. Similarly, the purpose of the gap between the two poles of the ring head structure is to define the recording transitions. Moreover, similar to a system with a ring head, a system utilizing a shielded writer can be utilized without any SUL at all. As shown in Figure 2.11b, the fairly small separation between the main pole and the shield provides sufficient efficiency. In most implementations, shields are coupled to the main pole through the back of the pole, as shown in Figure 2.11c. In this case, the trailing and cross-track side field gradients are determined by the flying height and the separation between the main pole and the shields rather than by the separation between the ABS and the SUL.

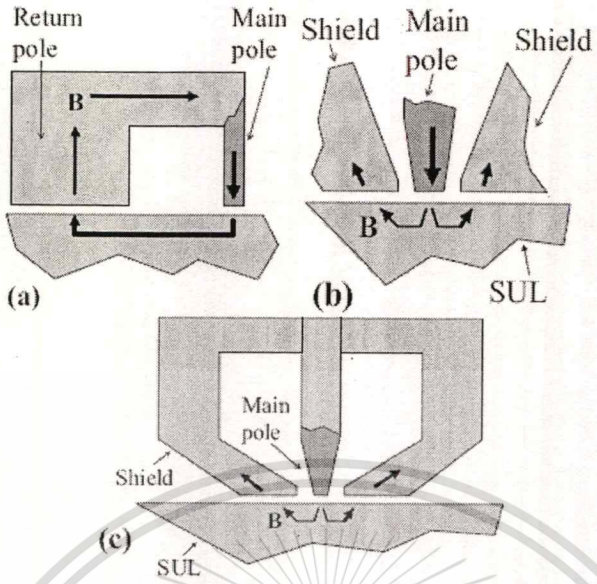

Figure 2.11 Diagrams showing the flux return paths in cases with a regular (a) SPH (along-track cross-section view) and (b) a shielded SPH (SSPH) (front view cross-section), respectively. (c) Full-scale front view cross section of SSPH [48]

In fact, for the considered dimensions, the only noticeable difference between the two modified systems, with and without a SUL, is the fact that the system without a SUL needs approximately 20 percent more current to saturate. To clearly illustrate the main dependence, the field is shown normalized to its saturation value. In summary, it can be concluded that the utilization of soft magnetic shields around the main pole results in the following advantages:

1) The recording field can be maintained to be fairly large (compared to the case without shields) with no substantial field gradient degradation at higher area densities.

2) The field gradient can be controlled via varying the separation between the main pole and each of the shields as well as by the pole tip and shield geometry.

3) If shields are used, the system efficiency could be increased through the reduction of the throat height. As a consequence, the skew angle sensitivity could be also substantially reduced.

2.2 Playback in Perpendicular Recording

Recent high areal density demonstrations of perpendicular recording clearly indicate an increasing interest in this technology [14-17]. It is believed that, as compared to conventional longitudinal recording, perpendicular recording is capable of deferring the superparamagnetic limit to a significantly higher areal density due to a thicker recording layer and/or the use of a soft underlayer (SUL) [18]. Although perpendicular recording is certainly the closest alternative to the conventional technology, its novelty also brings up new issues, not ever encountered in longitudinal recording. These issues have to be well understood before the technology can be fully and most efficiently implemented [19-21]. Major issues related to perpendicular media and perpendicular write heads have been previously considered [22-25]. However, relatively little attention has been given to the playback process. For example, the role of the SUL in the playback process is still an open question: although the SUL certainly increases the magnitude of the playback signal, its influence on the signal resolution is still controversial. Another fundamental source of the difference between the playback processes in longitudinal and perpendicular recording is the difference in the magnetic "charge" configuration in longitudinal and perpendicular media, respectively. Therefore, the intention of this Chapter is to investigate the physics of the playback process in perpendicular recording.

The physics of the playback process in perpendicular recording is explored. It is shown that due to the existence of the two layers of the "magnetic charge", at the top and effective bottom surfaces of the recording layer, the stray field sensed by a reader rolls off with the areal density essentially differently than it does in longitudinal recording. Unlike in longitudinal recording, in perpendicular recording, the recording layer thickness is an extremely sensitive parameter, which provides extra flexibility in controlling the density roll-off. It is illustrated that for areal densities beyond approximately 200 Gbit/in2, the slowest roll-off for both longitudinal and perpendicular recording occurs at a bit aspect ratio of 1:1. A fundamental role of the soft underlayer in the playback process is investigated. It is

illustrated that although at relatively low linear and track densities the use of a soft underlayer increases the playback signal, the signal does not depend on the use of a soft underlayer at high densities. It is shown that for both perpendicular modes, although at sufficiently low track densities (below ~ 50 ktpi), the signal disappears at relatively low linear densities, there is a significant non-zero signal even at zero linear density if the track density is sufficiently high (above ~ 300 ktpi). A magnetic image model is introduced to illustrate that the use of a soft underlayer could not improve the resolution of a recording system. Moreover, it is shown that there is range of the air-bearing-surface-to-soft-underlayer separation in which the playback resolution deteriorates. The guidelines are given on how to design a playback head to avoid the operation in the region of the deteriorated resolution. Besides the conventional playback head design including a single read element surrounded by two soft shields along the track, a number of other optimized for perpendicular recording designs are explored. For example, it is illustrated that compared to conventional single-read-element shielded configurations, differential reader configurations display superior playback properties in terms of both the playback amplitude and the spatial resolution.

The playback process is analyzed as not just a detailed study of another read head design but rather an integral process, including a reader and a medium. Such an integral consideration is especially critical for the perpendicular mode with a medium with a soft underlayer (SUL). In this mode, the SUL is often viewed as an indispensable part of the recording head. For broader and more insightful comprehension of the playback process in perpendicular recording, two analytic approaches, direct and reciprocity are considered. The "direct calculation" method addresses exclusively the fundamental contribution of a recording medium into the playback process. Thus, the fundamental issues related to the different "charge" configuration in a perpendicular medium could be more explicitly studied. As to the "reciprocity calculation," it reflects the magnetic properties of the playback head.

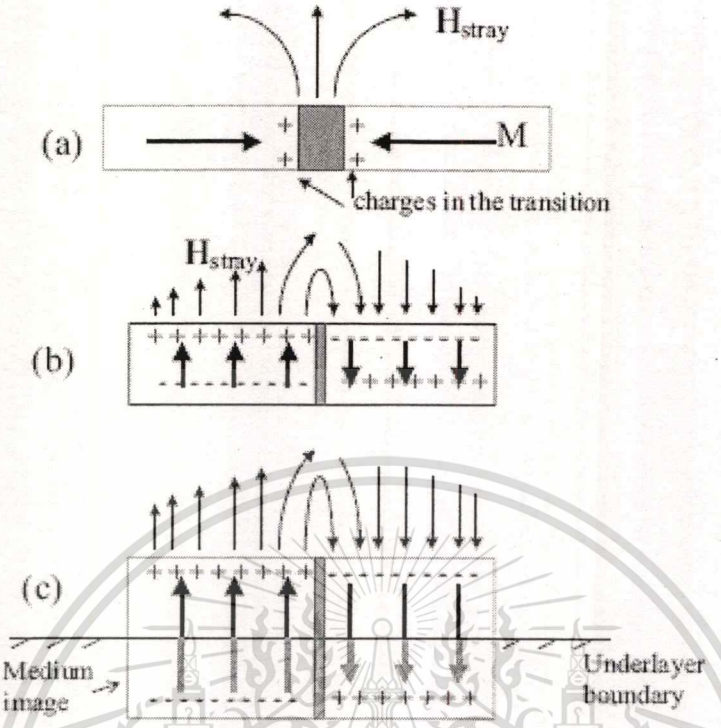

Figure 2.12 Diagrams showing the sources of stray fields in the case of (a) longitudinal recording, and perpendicular recording (b) without and (c) with a SUL [48]

To help understand the basic difference in the playback process between longitudinal and perpendicular recording, schematic diagrams of the stray fields emanating from a single transition in a longitudinal medium and a perpendicular media without and with a SUL are shown in Figures 2.12a-c, respectively [26]. As can be noticed, in the longitudinal case, the stray fields emanate only from the transitions, with the fields near the transitions oriented perpendicular to the disk plane. On the other hand, in the perpendicular cases, the stray field emanates from the effective "magnetic charge" at the top and effective (due to the SUL) bottom surfaces of the recording layer, with the field right above the transitions oriented parallel to the disk plane. In these calculations, the transition is assumed to be ideal. Also, in this example, for the description simplicity, infinitely wide tracks are

assumed. It should be noted that, in general, the stray field in the perpendicular cases looks similar to the stray field in the longitudinal case, provided that the perpendicular and in-plane components are interchanged. It is obvious that the effective distance away from the transitions, at which most of the drop in the stray field occurs, is determined by the effective recording layer thickness.

2.2.1 Examples of Reader Designs

The Reciprocity Principle is applied to analyze and compare four different reader designs (See Figure 2.13): a) unshielded reader [27]; b) shielded [28-29]; c) differential reader [30-33]; d) shielded differential reader [34]. Variations of shielded, differential, and shielded differential readers with the emphasis on various aspect of recording performance and manufacturability will be considered as well. Playback from a perpendicular recording medium with a soft underlayer and a single layer longitudinal recording medium will be investigated. For completeness, more exotic configurations such a longitudinal recording medium with a soft underlayer (keeper layer) and perpendicular recording medium without a soft underlayer will be considered as well.

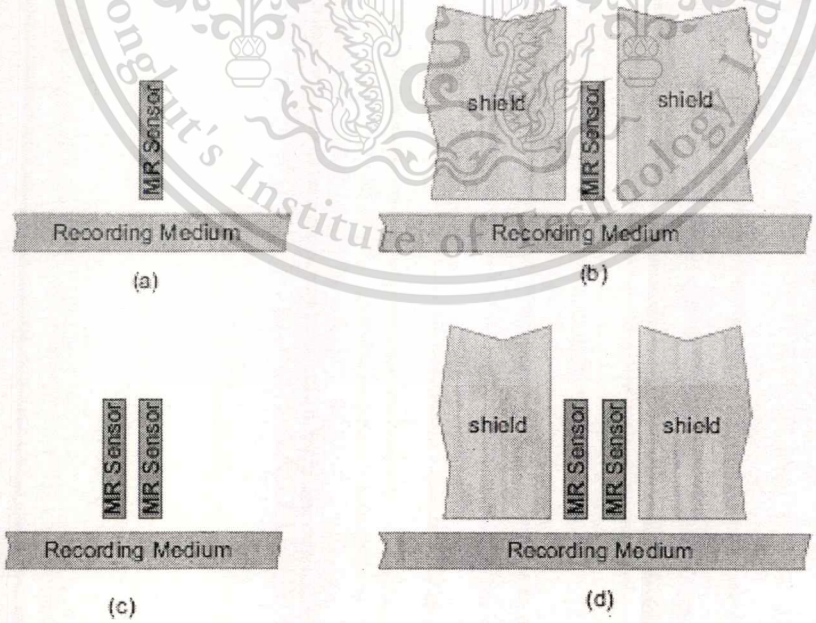

Figure 2.13 Schematics of various reader designs: a) unshielded reader, b) shielded reader, c) differential reader, d) shielded differential reader [48]

As mentioned earlier, the reciprocity principle is used to study playback performance of various readers [35-36]. The playback voltage of a linear playback head is equal to the convolution of the sensitivity field (function) of the reader with the magnetization pattern written into the recording layer. The sensitivity field is calculated as the field generated by the read-head, in which the read sensor is substituted with an equivalent soft magnetic material with a current carrying imaginary coil wrapped around [37].

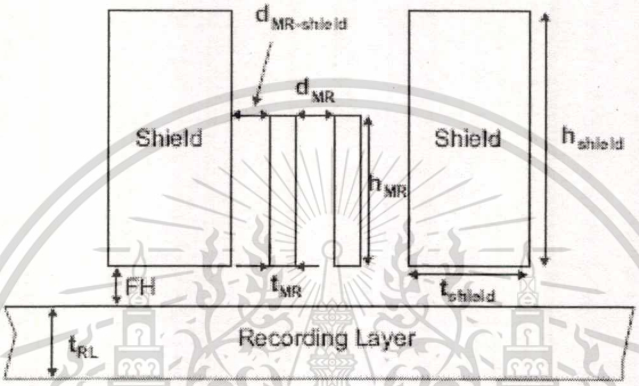

Figure 2.14 Schematic of a shielded differential reader with the relevant dimensions outlined [48]

The reader design parameters used in calculations are similar to the ones suggested by M. Mallary *et. al.* [38] for a 1Terabit/in2 perpendicular recording system design. Unless specified otherwise, the magnetic thickness of an MR sensor, t_{MR}, is assumed to be 10nm. The cross-track width of an MR sensor, w_{MR}, is 40nm. The height of the MR sensor, h_{MR}, is 40nm. The separation between the MR sensor and the shields, $d_{MR-shield}$, and the separation between the two MR sensors in differential designs, d_{MR}, are set to be 10nm each. The flight-height, FH, is 5nm and the media thickness, t_{RL}, is 10nm. The shields thickness, t_{shield}, is 100nm, the shield cross-track width, w_{shield}, is 400nm, and the shield height, h_{shield}, is 220nm. The dimensions mentioned above are shown in a schematic drawing of a shielded differential reader in Figure 2.14. The presence of an ideal soft underlayer is modeled with symmetric boundary conditions on the top surface of the soft underlayer. Magnetic field modeling based on boundary element approach is utilized throughout the chapter

2.2.2 Giant-magnetoresistive (GMR) heads

Sensor magnetism and magnetoresistanc.

As explained in detail else where in this issue, in magnetic multilayers the GMR signal comes from the change in electrical resistance that occurs when there is a change in the angle between two or more magnetic layers separated by a conducting spacer. In a standard GMR sensor as Fig. 2.15, the two magnetic layers are the reference layer (RL) and the free layer (FL). Typically, the resistance of the sensor is minimum when RL and FL are parallel (R = Rmin), while it is maximum when they are anti-parallel (R = Rmax = Rmin +ΔR), and varies as R = Rmin + (ΔR/2)(1 - cosø), where ø is the angle between the magnetizations.

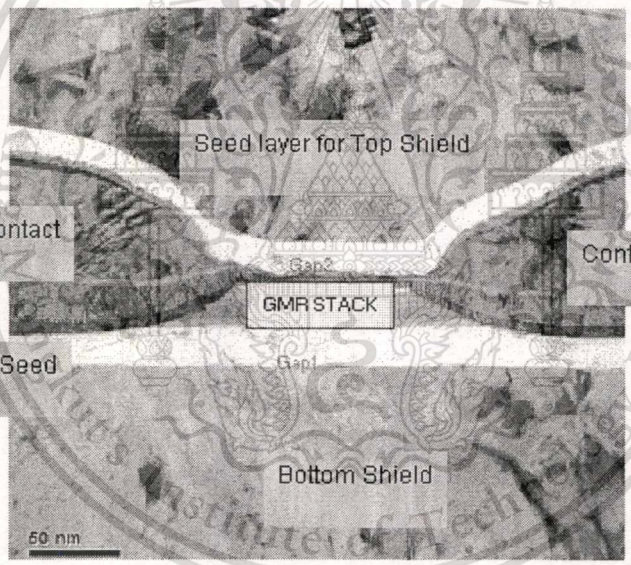

Figure 2.15 Disk-view schematic of typical thin-film multilayer stack for CIP GMR sensor. The current flows horizontally between the lead/hard bias regions [Seagate].

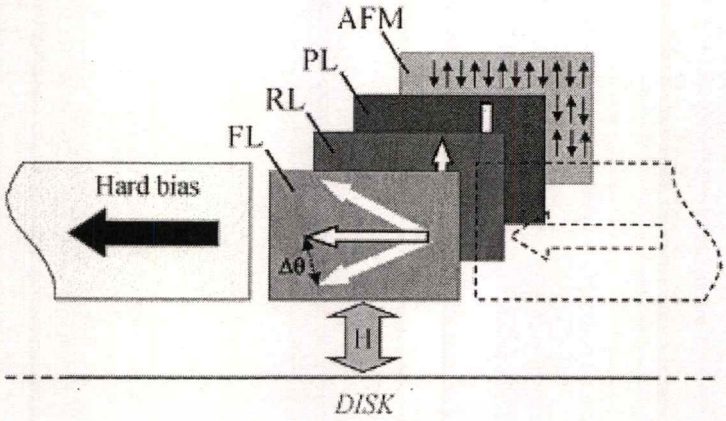

Figure 2.16 Perspective view of the relative magnetization directions of the Hard bias, free sensing layer (FL), reference layer (RL), pinned layer (PL), and pinning antiferromagnetic layer (AFM) for a typical GMR head. The signal transition fields H from the recorded media disk are oriented vertically. These relative orientations also apply to CPP-TMR or CPP-GMR heads [49]

The sensor output needs to be linear in order to optimize signal processing and reading density. Therefore the head is engineered so that the easy-axis of the free layer magnetization is oriented along the disk surface with a uniaxial anisotropy *H*k. The vector sum of hard bias fields, anisotropy fields, current-induced fields, demagnetization fields and interlayer coupling fields are such that in the zero-field state the FL and RL magnetizations are approximately perpendicular (ø = 90°). See Fig. 2.16. Angular deviations of the FL magnetization during read back due to the vertical component of the media magnetic field (Δø +/-30°) result in a quasi-linear output voltage [39]. While the quiescent direction of the FL magnetization is determined by the hard-bias direction, the magnetization direction of the reference layer is made to be 'pinned' by direct exchange coupling to an antiferromagnet (AFM). The strength of the exchange energy (typically *J*ex > 0.3 erg/cm2) at the ferromagnetic/antiferromagnet interface determines the degree of 'pinning' of the RL. This results in an effective pinning field which is inversely proportional to the reference layer magnetization and thickness: $H_{ex} = J_{ex}/M_{RL}t_{RL}$. To further improve the pinning of the RL, every sensor today employs the technique of antiparallel-pinned (AP-pinned) reference layer, where the RL is first exchange coupled to another

magnetic layer (the pinned layer PL) via indirect antiferromagnetic exchange mediated by a thin AP-pinning layer (APL) such as Ru [39]. Typically the thickness of Ru is tuned near the first negative (antiferromagnetic) peak of the oscillatory indirect exchange coupling (Ru = 8 Å), resulting in a strong coupling of *J*ex = 1 erg/cm2. Since the RL and the PL are strongly coupled antiparallel to each other, they form a rigid magnetic layer whose net magnetization $m_{AP} = M_{RL}t_{RL} - M_{PL}t_{PL}$ can be made arbitrarily small such that the exchange pinning field *H*ex = Jex/m_{AP} can be greatly increased. Just as important, this AP-pinning technique dramatically reduces the net magnetostatic demagnetization field generated by the RL when the sensor is fabricated to submicron dimensions, which otherwise interferes with proper stabilization of the sensor free layer. The magnetic response of the free layer is critical to sensor operation. The magnetic thickness of the free layer generally decreases with increased recording density since to achieve a given response (angular deviation $\Delta\phi$), the free layer moment must be matched to the media flux density (*M*r x *t* where *M*r is the remnant media magnetization and *t* is the media thickness). The media thickness generally scales inversely with recording density, reducing the optimal free layer thickness. With decreasing data bit size, the sensor must also fly closer to the disk to achieve the required resolution. To optimize the overall properties, the free layer is typically a bilayer of CoFe/NiFe*x*, where the Co_{90-60} Fe_{10-40} provides favorable interface to the Cu spacer layer, while the NiFe*x* layer (x <0.2) is chosen to reduce and control the intrinsic coercive field *H*c, magnetic anisotropy *Hk* and the magnetostriction *Y* of the sense layer.

2.3 Conclusion of literature review and fundamental of recording head

In this chapter, recent works on the recording heads between Internal Shunting and Non Internal Shunting have been reviewed through fundamental of ESD. Previous studies were really helpful in understanding the principles of load resistance limitation, ESD behavior and the anti-static robustness enhancement with internal shunting head. A simple lumped RLC model for a hard disk drive is developed and used in SPICE circuit simulations. Simulation results were compared with experimental measurements using a special "hybrid" disk drive to validate the SPICE model. The voltage on and between the head and disk inside the drive were

modeled during an ESD event to the base plate and/or disk. Experimental measurements and SPICE modeling show that if the disk grounded when there is a large disk-to-base resistance, then head-to-disk electrical breakdown can occur. It is concluded that an electrical model is valuable in developing an understanding of the effects of ESD on a hard disk drive. The effect of the GMR sensor resistance on HBM and MM ESD current waveforms is studied. It is shown that the sensor resistance can have a significant impact on the peak current and waveform shape, especially for MM ESD testing. The conventional shunting by tab process may cause the damage of GMR heads due to the raised voltage between the GMR sensor lead and the bottom shield. However, after completing the HGA production, the shunt leads have to be trimmed in order to test its electrical characteristics. This is thought to cause the ESD effect while trimming the shunt tab. Internal shunting is introduced on tunneling magnetoresistive heads to enhance device anti-static robustness and external high-frequency noise pickup immunity. The details of the shunting scheme and the mechanism leading to both anti-static robustness and reduced high-frequency noise pickup are discussed.

CHAPTER 3

Fundamental Concepts of Electrostatic Discharge (ESD)

3.1 Device Response to External Events[46]

On the first issue of preventing any physical element in the system from latent or permanent damage that impacts the functionality, reliability, or quality from ESD events, there is significant misunderstanding. It is a belief of many engineers that the objective of the ESD networks is to carry all of the ESD current, as well as be the first element to undergo failure. It is also a belief that it does not matter if the ESD structure undergoes failure. These statements are not accurate understanding of the objective of ESD design. The role of the ESD network is to increase the ESD robustness of the complete product or application. The ''failure criteria'' is based on the functional, reliability, or quality objective of the electrical component. In ESD design, the ESD devices as well as the circuits, which are to be protected, can be designed to respond to (and not to respond to) unique ESD current waveforms. In standard circuit design, digital circuits are designed to switch from logic state levels, rising or falling edges. Circuits can store information or mix different logical states. ESD networks typically are designed to respond to specific ESD pulses. These networks are unique in that they address the current magnitude, frequency, polarity, and location of the ESD events. Hence, in ESD design, the ESD networks are designed and tuned to respond to the various ESD events. In ESD design, different stages or segments of the network can also be designed to respond to different events. For example, some stages of a network can respond to human body model (HBM) and machine model (MM) events, while other segments respond to the charged device model (CDM) event. These ESD events differ in current magnitude, polarity, time

constant, as well as the location of the current source. Hence, the ESD circuit is optimized to respond and address different aspects of ESD events that circuits may be subjected to. Additionally, circuits can be modified to be less sensitive to ESD events using ESD circuit techniques. As a result, the understanding of the material, device, circuit, and system physical time constants is critical in ESD design.

3.2 ESD event

3.2.1 ESD time constants

To understand physical phenomena, and particularly ESD phenomenon, it is necessary to quantify the scale in both space and time. ESD phenomena involves microscopic to macroscopic scales. ESD phenomena involve electrical and thermal transport on the scale of nanometers, circuits and electronics on the scale of micrometers, semiconductor chip designs on the scale of millimeters, and systems on the scale of meters. The time scales of interest range from picoseconds (ps) to microseconds (us). Electrical currents of interest range from milliamps (mA) to tens of amperes (A). The voltage range of interest varies from volts (V) to kilovolts (kV). Temperatures vary from room temperature to melting temperatures of thousands of degrees Kelvin. It is the vast ranges of time, space, currents, voltages, and temperature as well as its transition from the microscopic to the macroscopic, which makes ESD phenomenon difficult to model, simulate, and quantify. To comprehend ESD phenomenon and establish validity of analytical developments, it is important to be able to understand what phenomenon is important. By analyzing the physical equations from a time constant approach, equations and understanding can be made both rigorous as well as improve logical clarity.

3.2.2 ESD events

To understand the role of ESD events and the physical environments, it is important to quantify the characteristic times of an ESD event. ESD events are represented as circuit equivalent models. Figure 3.1 contains the ESD time constant hierarchy.

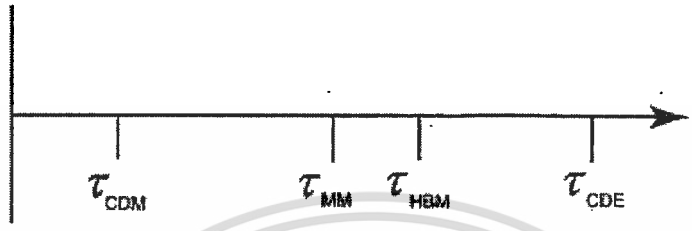

Figure 3.1 Electrostatic discharge (ESD) time constant hierarchy [46]

3.3 Capacitance, Resistance, Inductance and ESD

3.3.1 The Role of Capacitance

In the understanding of ESD events, it is important to understand the role of capacitance, resistance, and inductance and where it comes into play in the analysis. Capacitance has a role in the capacitive loading effects in networks, timing circuits, as well as charge storage, charge distribution, and displacement current in ESD events. In ESD design, capacitance has a role in the following environments:

- Capacitance loading effects of ESD protection networks for signal pads.
- RC-discriminator networks for frequency-dependent trigger networks for signal and power pads.
- Current distribution within an ESD network at high speed and radio frequency (RF) GHz applications.
- Current distribution within a chip power rails and power grid.
- Chip or system impedance
- LC transmission lines for RF applications.

Capacitance loading effects are a concern for receiver networks because it impacts circuit performance objectives. As the application frequency increases, circuit designs desire to lower the ESD input network capacitance loading. For example, in some applications it is desired to maintain a constant reactance, then as the functional frequency increases, the ESD loading capacitance decreases accordingly. Capacitance also plays a role in trigger networks, which tune the RC time constant so that the ESD network responds to the ESD pulse. Circuits are designed to respond to the ESD impulse but not to the power-up or functional frequencies, discriminating the response to ESD events instead of functional applications.

For RF applications, the role of the capacitance influences the frequency response of the ESD network as well as its location on a Smith Chart. Capacitance also plays a role in the way in which current distributes through a semiconductor chip power grid. The capacitance per unit distance of the power bus plays a role in how the current distributes within a semiconductor chip. Capacitance plays a role in the impedance (or effective impedance) of the whole chip. The chip or system impedance plays a key role in the ability to displace current across the chip. In RF applications, capacitance plays a role in the LC transmission line elements used in RF applications. Hence, the understanding of lumped and distributed capacitance is fundamental in ESD events. Capacitance is key from the local ESD element, circuits as well as the global capacitance components of a semiconductor chip. It can be observed locally within a semiconductor device, a circuit or globally on a chip level.

3.3.2 The Role of Resistance

Resistance is one of the most important parameter in ESD events. The role of resistance is critical in the voltage and current distribution within a semiconductor device, circuit, or network. The understanding of resistance and the resistance distribution plays a more significant role compared to inductance and capacitance

issues. Typically, inductance plays an important role in the effect of lead frames and packages on the ESD response, but play a minor role in the understanding of ESD devices and circuit response in semiconductor chip environments. Capacitance also plays a key role when the RC time of the wiring is of the order of the characteristic time of the event. Hence, the understanding of lumped and distributed resistance systems is fundamental in ESD events. In ESD design, resistance has a role in the following environments:

- Voltage distribution and on-resistance within an ESD protection structure.
- Voltage distribution and on-resistance within the protected circuit.
- Voltage and current distribution through the power grid.
- Voltage and on-resistance of the ESD power clamps.
- RC-discriminator networks for frequency-dependent trigger networks for signal and power pads.
- Current distribution within an ESD network at high speed and radio frequency (RF) GHz applications.

Resistance plays a fundamental role in the operation of an ESD protection circuit. Voltage distribution and on-resistance within an ESD protection structure is critical in order to provide an effective ESD structure. Additionally, the resistance also plays a role in the Joule heating within the ESD structure. The voltage distribution and on-resistance within the protected circuit is also critical in the understanding of the failure of an ESD network. The voltage and current distribution through the power grid is critical in that it influences the peak voltage and current in the system. These factors can drive the effectiveness of the ESD strategy, and can determine power clamp circuit placement. In the ESD power clamps, the net resistance also plays a role in the ESD event. The resistance of the power grid also decreases the voltage margin between the ESD current path and the voltage at the protected circuit of

interest. Hence, the understanding of lumped and distributed resistance is fundamental in ESD events. Resistance is key from the local ESD element, circuits as well as the global capacitance components of a semiconductor chip. It can be observed locally within a semiconductor device, a circuit, or globally on a chip level.

3.3.3 The Role of Inductance

In the understanding of ESD events, it is important to understand the role of inductance and where it comes into play in the analysis. Inductance has a lesser role compared to resistance and capacitance effects. Inductance primary role occurs in package lead frames, wire bonds, package pins, and the package itself. In analog and mixed signal (A&MS), RF CMOS, and RF BiCMOS applications, inductors are used in circuits for dc-biasing and blocking, LC transmission lines, LC tank circuits, and other RF circuit applications. In ESD design, inductance has a role in the following environments:

- Packaging lead frames.
- Package wire bonds.
- Package pins.
- RF circuit elements—LC transmission lines.
- RF circuits with dc-biasing.
- RF ESD circuits.

Package lead frames and wire bonds can influence the inductive coupling between power rails and influence circuit response. To reduce the on-chip noise, power rails are reconnected at the package lead frame, or pads, or at the package. In this fashion, the package inductance plays a role in the response of peripheral circuits which have disconnected power and ground rails on the chip. Inductance is also playing a more critical role with the introduction of inductors and transmission lines

as design elements. Inductors are used in dc-biasing networks, LC tank circuits and are being introduced into ESD networks. Inductors are being introduced to provide distributed networks isolated for lowering the effective loading of ESD elements. As a result, the understanding of lumped and distributed LC transmission lines is key to understanding the effect of inductance on ESD events. Hence, the understanding of lumped and distributed inductance is fundamental to ESD understanding in packaging and RF applications.

3.4 A Time Constant Approach

To comprehend ESD phenomena, and establish validity of analytical developments, it is important to be able to understand what phenomenon is important. By analyzing the physical equations from a time constant approach, equations and understanding can be made rigorous, as well as improving logical clarity. In such a fashion, electrical and thermal phenomena can be understood. By familiarity with the important time constants of interest, our understanding as well as insight will be better served. It is through this process that one can establish a higher intuition in this complex field.

To understand the role of ESD events and the physical environments, it is important to quantify the characteristic times of an ESD event. ESD events are represented as circuit equivalent models.

3.4.1 ESD Time Constants

To understand physical phenomena, and particularly ESD phenomenon, it is necessary to quantify the scale in both space and time. ESD phenomena involve microscopic to macroscopic scales. ESD phenomena involve electrical and thermal transport on scale of nanometers, circuits and electronics on the scale of

micrometers, semiconductor chip designs on the scale of millimeters, and systems on the scale of meters. The time scales of interest range from picoseconds to microseconds. Electrical currents of interest range from milliamps to tens of amperes. Voltages range of interest varies from volts to kilovolts. Temperatures vary from room temperature to melting temperatures of thousands of degrees Kelvin. It is the vast ranges of time, space, currents, voltages, and temperature as well as its transition from the microscopic to the macroscopic which makes ESD difficult to model, simulate, and quantify.

3.4.2 Human body model characteristic time

A fundamental model used in the ESD industry is known as the human body model (HBM) pulse. The model was intended to represent the interaction the electrical discharge from a human being, who is charged, with a component, or object. The model (Figure 3.2) assumes that the human being is the initial condition. The charged source then touches a component or object through a finger. The physical contact between the charged human being and the component or object allows for current transfer between the human being and the object. A characteristic time of the human body model is associated with the electrical components used to emulate the human being. In the HBM standard, the circuit component to simulate the charged human being is a 100 pF capacitor in series with a 1500 ohm resistor. This network has a characteristic rise time and decay time. The characteristic decay time is associated with the time of the network where R_{HBM} is the value of the series resistor and C_{HBM} is the charged capacitor. This is a characteristic time of the charged source. The HBM characteristic time constant is physically interesting since the time of the pulse is of the order of the thermal diffusion time of many materials used in the semiconductor industry.

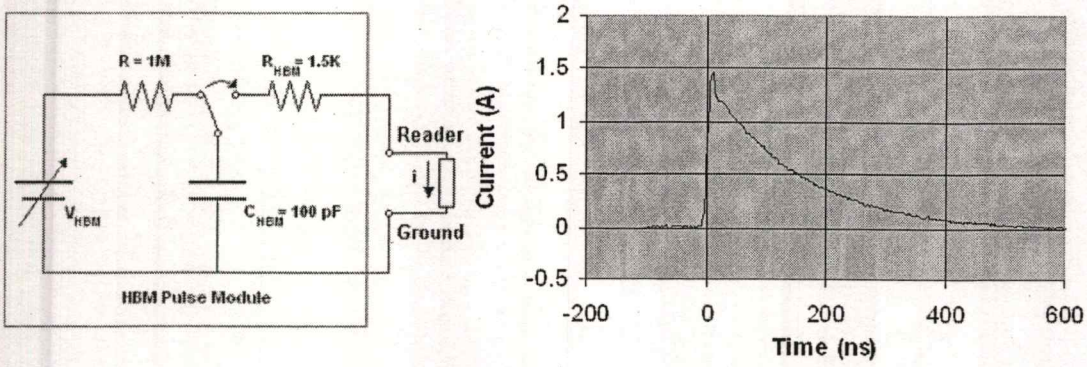

Figure 3.2 Human body model equivalent circuit [46]

3.4.3 Machine model characteristic time

Another fundamental model used in the ESD industry is known as the machine model (MM) pulse [39]. The model was intended to represent the interaction the electrical discharge from a conductive source, which is charged, with a component, or object. The model assumes that the 'machine' is charged as the initial condition.

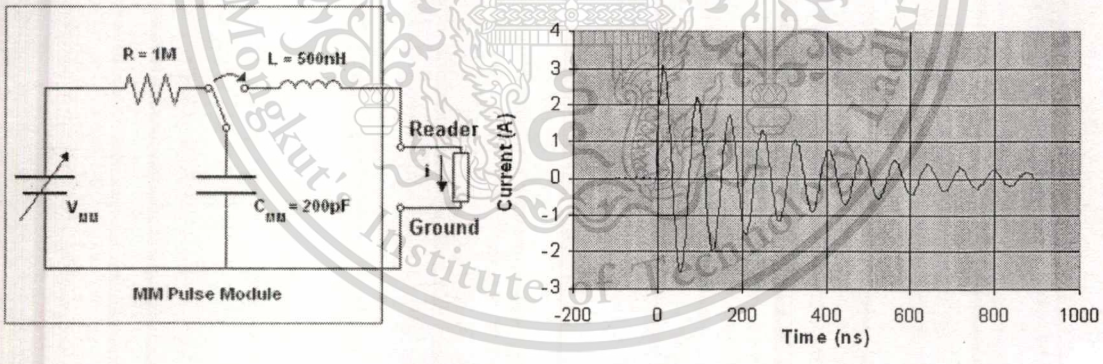

Figure 3.3 Machine model equivalent circuit [46]

The charged source then touches a component or object. In this model (Figure 3.3), an arc discharge is assumed to occur between the source and the component or object, allowing for current transfer between the charged object and the component or object. A characteristic time of the machine model is associated with the electrical

components used to emulate the discharge process. In the MM standard, the circuit component is a 200 pF capacitor with no resistive component. An arc discharge fundamentally has a resistance of the order of 10–25 ohm The characteristic decay time is associated with the time of the network

$$T_{MM} = R_{MM}C_{MM}$$

where R is the arc discharge resistor and C is the charged capacitor. This is a characteristic time of the charged source. The MM characteristic time scale is significantly faster than the HBM characteristic time scale, due to the lack of a resistive element. The MM response is oscillatory and has significantly higher currents than the HBM ESD event. Experimentally, MM ESD protection level magnitudes are typically 5–10 times lower than HBM ESD protection level magnitudes.

3.4.4 Charged device model characteristic time

The charged device model (CDM) represents an electrostatic discharge interaction between a Head and a discharging means where the Head is pre charged. The charging process can be initiated by direct charging, or field-induced charging. The discharge process is initiated as contact is initiated between the charged device and the discharging means. CDM discharge occurs at less than 5 ns where typically the rise time of the event is of the order of 250 ps. The CDM event is the fastest of the ESD phenomena, and occurs on a time scale significantly faster than thermal diffusion properties, and of the order of the modern electronic circuit response times. As a result, the response is near the thermal adiabatic assumption for the materials used in semiconductors.

3.5 Conclusion of ESD to recording head.

Magnetoresistive (MR) and giant MR (GMR) sensors are used in magnetic recording as read transducers and it is well known that they are highly susceptible to damage from electrostatic discharge (ESD). It is therefore highly valuable to characterize the

ESD damage thresholds and failure mechanisms of these devices by doing human body model (HBM), machine model (MM) and direct charged device model (DCDM) testing. The HBM ESD test method shown in Fig. 3.4 is a well-known test method for ESD stressing.

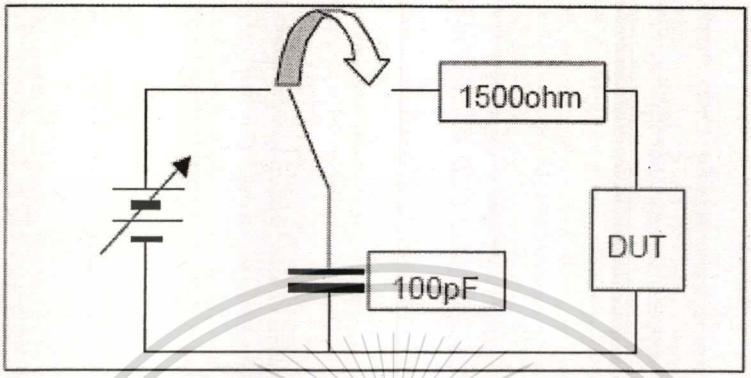

Figure 3.4 HBM circuit diagrams [4]

A 100pF capacitor is charged to a desired voltage and then discharged through a 1500ohm resistor to the device under- test (DUT). Generally, the GMR sensor resistance ranges from 35ohm to 50ohm, so the 1500ohm resistor in the tester dominates the load resistance. Therefore, the effect of GMR head resistance on the waveform is expected to be small. However, for the MM ESD test shown in Fig. 3.5 the capacitance is 200 pF and there is no significant tester resistance in the discharge circuit path. Therefore, the effect of the GMR head resistance could be significant during MM ESD testing. Surprisingly, little consideration has been given in the literature to the effect of the sensor resistance on the current waveform, and hence the failure voltage and current. The purpose of this study is to demonstrate that the sensor resistance can have a profound impact on the current waveform shape, especially for MM ESD testing. This is important to understand when testing devices that vary significantly in resistance. An example of such a case would be ESD testing of higher resistance GMR or tunneling MR (TMR) devices.

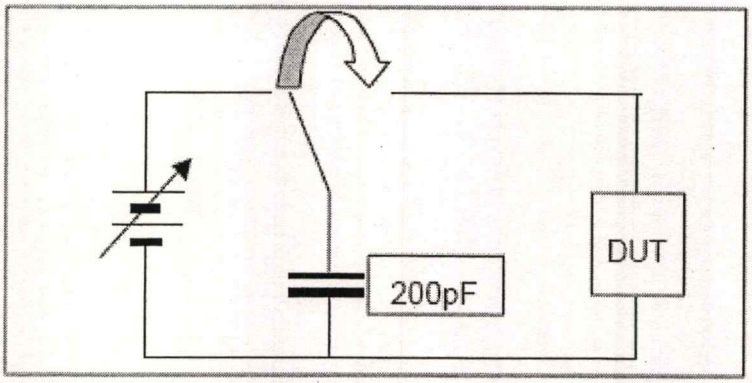

Figure 3.5 MM circuit diagrams [4].

HBM and MM ESD testing were performed on bottom spin-valve GMR sensors using an Integrated Solutions Int'l (ISI) QST-2001 QST tester. The transient current waveform was captured using a Tektronix CT-6 current transformer (2 GHz) and a LeCroy 4396 digital oscilloscope (1.5 GHz). Figure 3.6 shows examples of the measured HBM and MM current waveforms. We define the ESD transient current on each pulse is the difference between 1st over peak value to 1st under peak value.

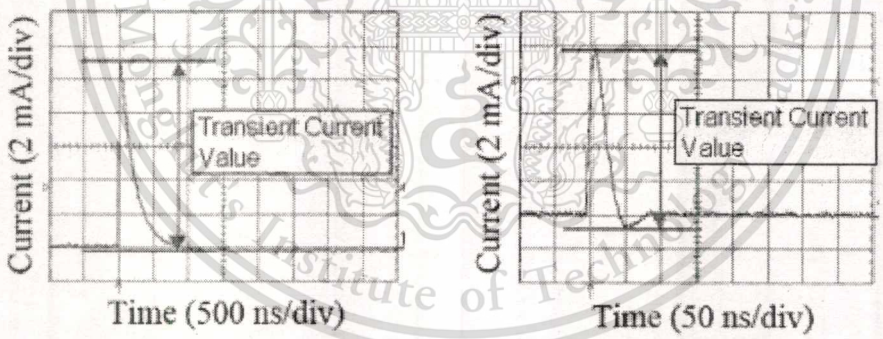

Figure 3.6 HBM (left) and MM (right) current waveforms [4].

During testing, the charging voltage was increased in small steps and the waveform of discharge transient current was captured along with the quasi-static transverse curve after each current pulse.

CHAPTER 4

Design of Experiment

4.1 Motivation of experiment

Figure 4.1 shows a typical magnetic recording hard disk drive (HDD) with the cover off that is used in desktop computers to store information, as well as an exploded view of the main components inside a drive. The main components are the printed circuit board, base, spindle motor, disk, and head stack assembly (HSA). Each subassembly in turn consists of additional components. For example, the HSA consists of the arm, voice coil, interconnects, preamplifier and of course the ultra-ESD-sensitive GMR magnetic recording head on the slider. While the ESD sensitivity of each individual component and some subassemblies is well known, the ESD sensitivity of the assembled disk drive system is largely unknown, except for two special cases. It is important to understand the ESD sensitivity of an assembled disk drive because of the possibility of new ESD failure modes when two or more individual components or subassemblies are combined together inside the HDD. A prime example of this is when the heads on an HSA are loaded onto the disk, resulting in the possibility for electrical breakdown between the slider or GMR sensor and the disk.

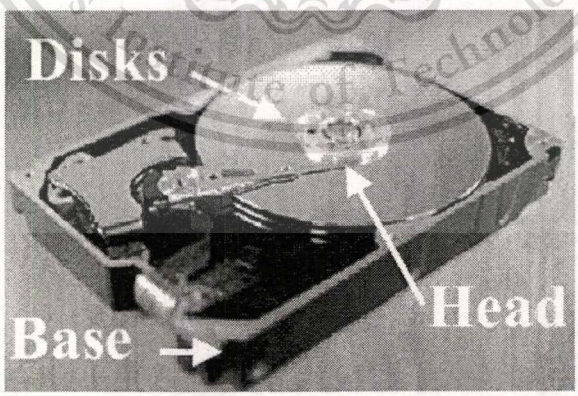

Figure 4.1 Photo of a typical hard disk drive with 3.5inch disks. Note that the cover has been removed, revealing the disks and recording head [Seagate]

TMR sensors are used in magnetic recording as read transducers and it is well known that they are highly susceptible to damage from ESD. It is therefore highly valuable to characterize the ESD damage thresholds and failure mechanisms of these devices by doing human body model (HBM), machine model (MM) and direct charged device model (DCDM) testing [45][46]. This study is carried out on high risk ESD items at the process [47] while being produced the HGA, including of any automated or manual operations in HGA process which involve direct contact to MR element, such as HGA assembly process and testing process as shown in Fig 4.2

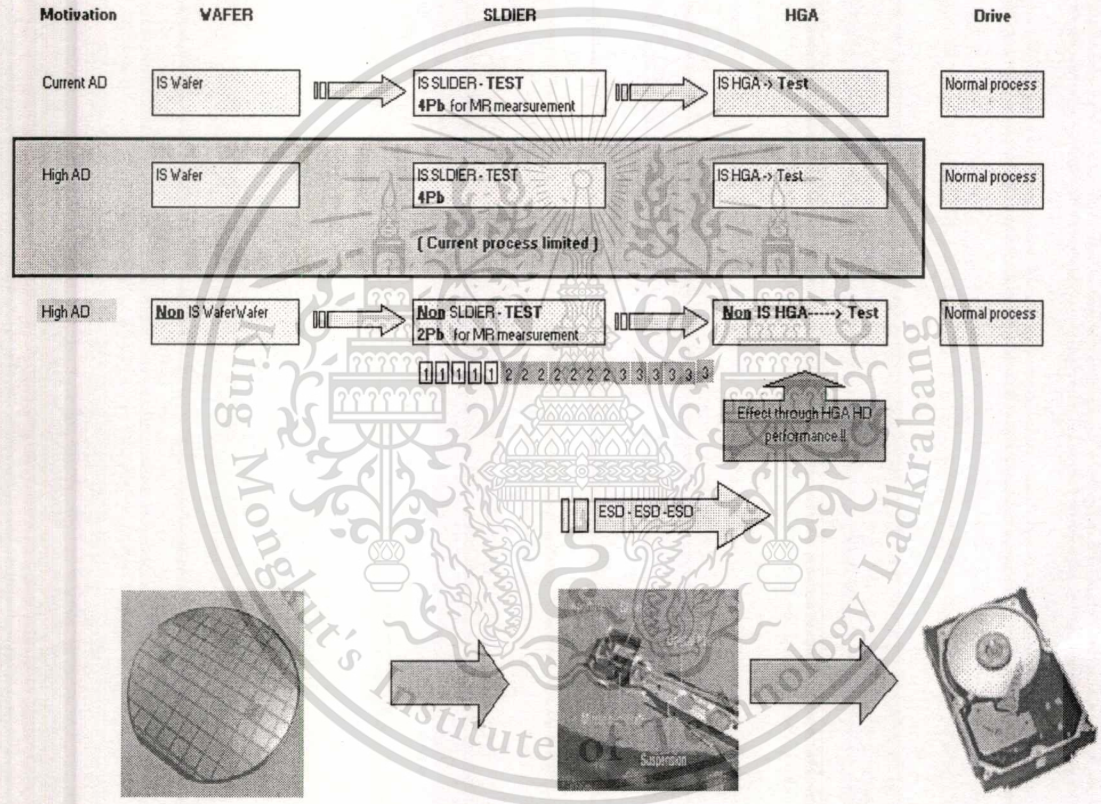

Figure 4.2 Process flow of Wafer through Drive

Due to its scaling error for MR resistance measurement, multi-4pt probing [43] is required for ISI [44] slider test to maintain test accuracy. Fig. 4.3 shows sliders with multiple pads, (a) for low areal density (AD) and (b) for high areal density. Comparing both of the sliders, the pad size of the high areal density slider is 40% smaller than that of low areal density slider. Because of its smaller pad size, measurement with

4pt probing technique on the high areal density slider can result in large amount of error.

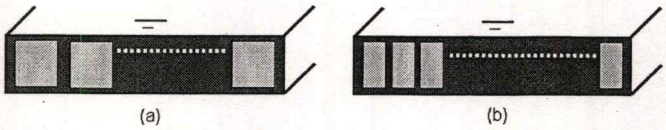

Figure 4.3 Slider with multiple pad (a) for low areal density media (b) For high areal density media

Sizes of probe tips used in 4pt probing and pads of the low areal density slider and the high areal density slider are illustrated in Fig.4.4

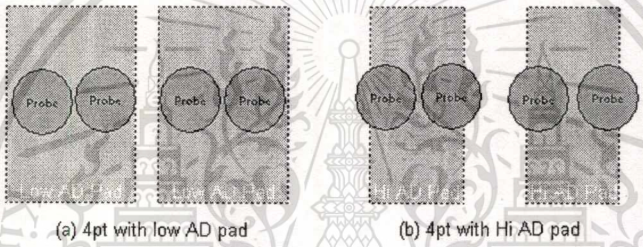

Figure 4.4 Probe 4pt Tip to slider pad comparison of low areal and high areal density slider

Since the non-IS design requires only 2pt probing, therefore, each pad needs to accommodate only one probe tip. As a result, the non-IS design is suitable for the smaller pad size of the high areal density slider as shown in Fig. 4.5 Consequently, this design is being considered for new coming recording head.

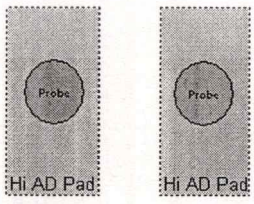

Figure 4.5 Probe 2pt Tip to slider pad of high areal density slider

4.2 Sample selection for thesis study and key parametric performances

For any experimental evaluation, the sample selection is one of the key criteria and so for this evaluation too. The samples used in this thesis study were all from regular manufacturing process from the Seagate. Although these samples are from regular manufacturing process, they were all fabricated to test the read back signal. Representing the full distribution are to avoid the bias of the sample values.

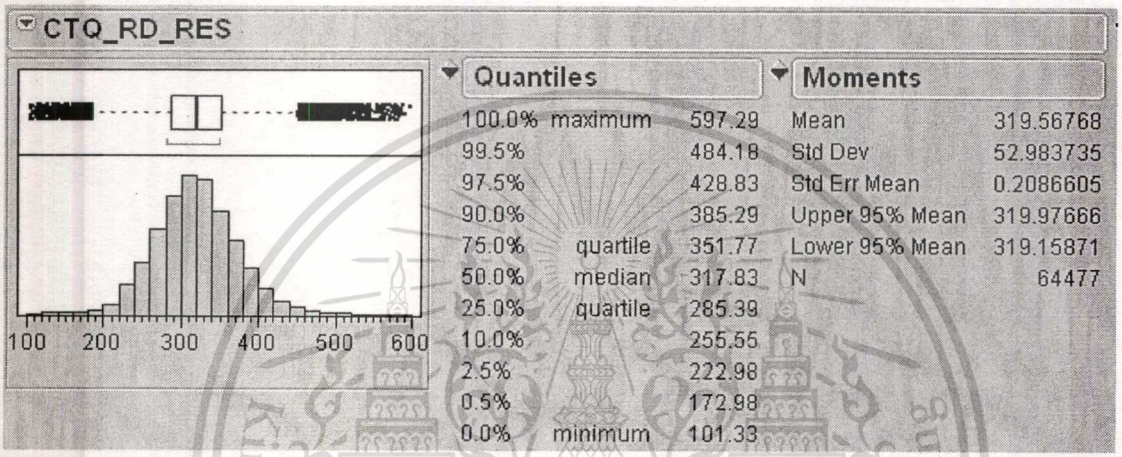

Figure 4.6 Reader resistance distributions of the samples before selection

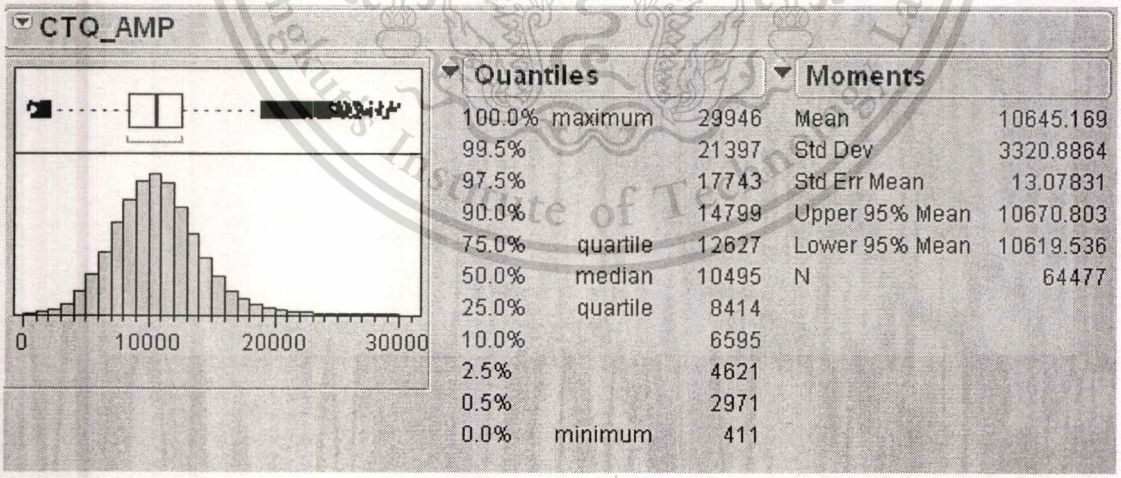

Figure 4.7 Read back amplitude distributions of the samples before selection

Fig 4.6 and Fig 4.7 illustrates the normal distribution of the evaluation samples before selection. From the graph of Fig 4.6 we could see that the reader resistance

population varies from 100 to 600 ohm from 64,477 samples. Fig 4.7 we could see that the read back amplitude population varies from 400 to 25mV. (Graph is micro Volt).

4.3 Evaluation setting

4.3.1 1st evaluation is quick check for head performance verification

It is head performance comparison between IS vs non IS HGA to see read back signal (reader resistance and amplitude) performance is using Electrical Tester Spin Stand (ETS) tester. The focus is on the fundamentals and applications of spin stand ET tests that may be used in development and mass production phases in the factory environments. Head Gimbal Assembly (HGA) is using Perpendicular Magnetic Recording in the full range of reader resistance and read back amplitude each group is 2,900 HGAs. The details require for evaluation are as below details.

1. Human Body Model (HBM) is control.
   1.1 Body voltage (resistance) monitoring of personnel.
2. Machine Model (MM) is control.
   2.1 Ensure all conductors that contact sensitive devices are grounded.
   2.2 Voltage measurements on isolated (non ground) conductors.
3. Direct Charged Device Mode (DCDM) is control.
   3.1 Voltage measurements on conductors as they move through the process.
4. Perpendicular recording granular Media with soft under layer (SUL) with current design of thickness and the recording layer coercivity.
5. Seagate ETS tester (HGA based dynamic electrical tester) with the high-performance servo improvement package (SIP).
6. The commercially available iterative channel.
7. Statistical analysis tool "JMP" and " Minitab " software is used for the analysis.

4.3.2 2nd evaluation is 400 Hours reliability test by Vermit reliability tester

Fig, 4.8 shown reader voltage stress Vermit test system. The failure caused at elevated stress level is the same mechanism at use level (lower stress), reli statistics. Elevated stress levels set to acquire enough data over 2-3 weeks period to predict reliability. Time to Failure (TTF) vs Stress is plotted by specifying the Life-Stress model (Arrhenius function) using reliability analysis software. The sample 128 sample HGAs / group of IS and Non IS head.

1. Life Test Temp and Tool: 85°C in Vermit 4 [Seagate]
2. Test Time: ~400 – 660 hours Thailand
3. Stress levels: Vary from 0.2~0.35V, 8 step
4. Life Analysis: ALTA PRO,
5. Failure Criteria: 30% MR change.

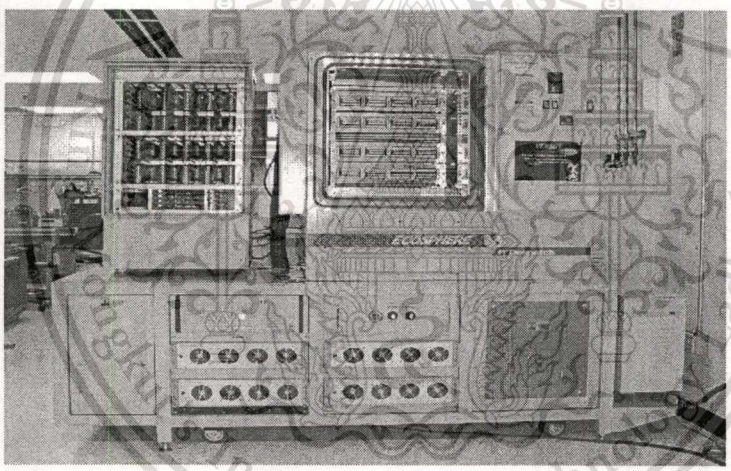

Figure 4.8 Reader Voltage Stress Vermit test [Seagate]

4.3.3 3rd evaluation is blown shunting at difference time (short 1 msec., medium 10 msec. and long time 100 msec.) on IS head

1. Compare read back IS of each blow time difference (short, medium and long time) on ETS tester. The samples are 128 sample HGAs per/group.
2. Compare 400 Hrs reliability test of each blow time difference (Short, Medium and long time) on Vermit the samples are 128 HGAs sample per/group. There are 8 steps of stress levels. It is vary from 0.2-035 V.

CHAPTER 5

Results and Conclusions

Electrical Tester Spin Stand (ETs) tests for the write and readability of the recording using the available heads in the manufacturing process have been investigated. Process for shunt removal at testing to recording head is at HGA ETs before the head is tested on the disc, the tester heater-controller circuits are programmed to apply a voltage pulse of 3.5V/100 msec. to the heater; the preamplifier diodes sink the fuse current. The opened fuse-link ends are separated by melted alumina, achieving a near-infinite permanent resistance. Fig 5.1 represents the schematic diagram of recording head and process for shunt removal at testing to recording head.

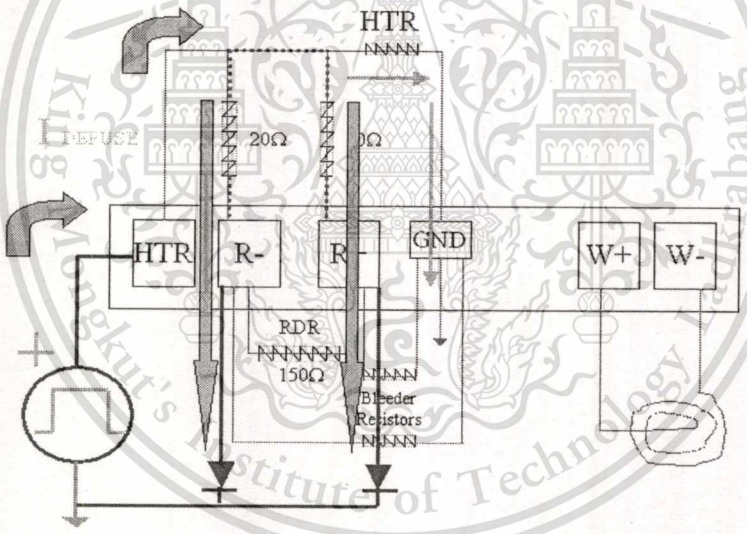

Figure 5.1 IS Head at HGA Tester – Shunt Removal [Seagate]

5.1 Head performance comparison between IS and Non IS HGA

First evaluation is to quick check for head performance verification. Using the IS vs non IS HGA to see read back signal performance (reader resistance and amplitude) is using ETs tester. Head gimbal assembly using Perpendicular Magnetic Recording in the full range of reader resistance and read back amplitude each group is 2,000 sample HGAs. Compare IS and non IS on head resistance (MR) and readout signal

amplitude (Amp) of IS and non-IS. The readout signals are measured at the beginning and at the end of the assembly process to see for performance change. These parameter metrics are used to determine the failure by percentage of the design due to ESD according to the target specification as shown in table 5.I.

Metrics	Conditions for Failure	Significate criteria of defective	Percent of Failure		Comment
			Non-IS	IS	
Delta R	>10% resistance	0-10%	2.16%	6.63%	acceptable
R	< Min. or > Max.	0-2%	0%	0.21%	acceptable
Delta Amp	>10% amplitude	0-10%	6.08%	0.89%	acceptable
Cum		0-10%	8.24%	7.73%	acceptable

Table 5.1 Compare defective of Non IS and IS

Table 5.1 shows cumulative failure by percentage. The IS has slightly lower cumulative yield (percent of failure) than non-IS, 7.73% vs. 8.24%, but it does not show a significant difference. Non-IS have lower delta resistance failure and higher amplitude failure than IS do. It is notice that ETS for evaluation set is different. The hierarchy of IS is to be arranged in order of resistance, amplitude and asymmetry. The hierarchy of non IS is to be arranged in order of amplitude, resistance and asymmetry. The parameter failure follows hierarchy test sequence. The ETs setting between IS and non IS is limited as ability of tester. It was set with difference hierarchy. Then, Considered cumulative yield is compared for both groups performance.

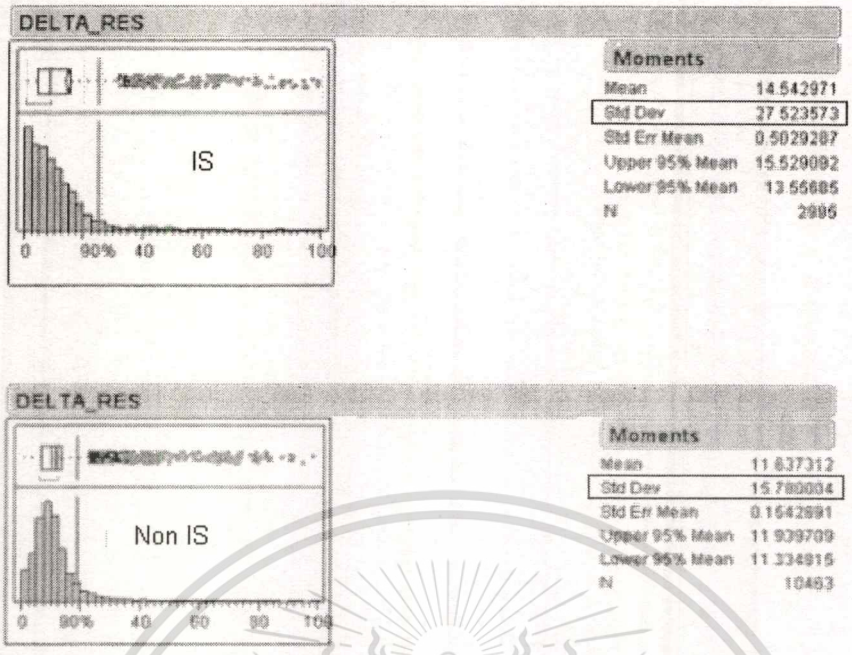

Figure 5.2 Delta reader resistance distribution of IS and Non IS

The parameter distributions were compared by mean and sigma. Fig. 5.2 compares the delta reader resistance of IS to Non-IS. Delta resistance failure corresponds with delta resistance sigma. The highlighted sigma values are in the distribution charts. This is a one-sided distribution. An inflated distribution tail in this case causes the higher sigma for IS

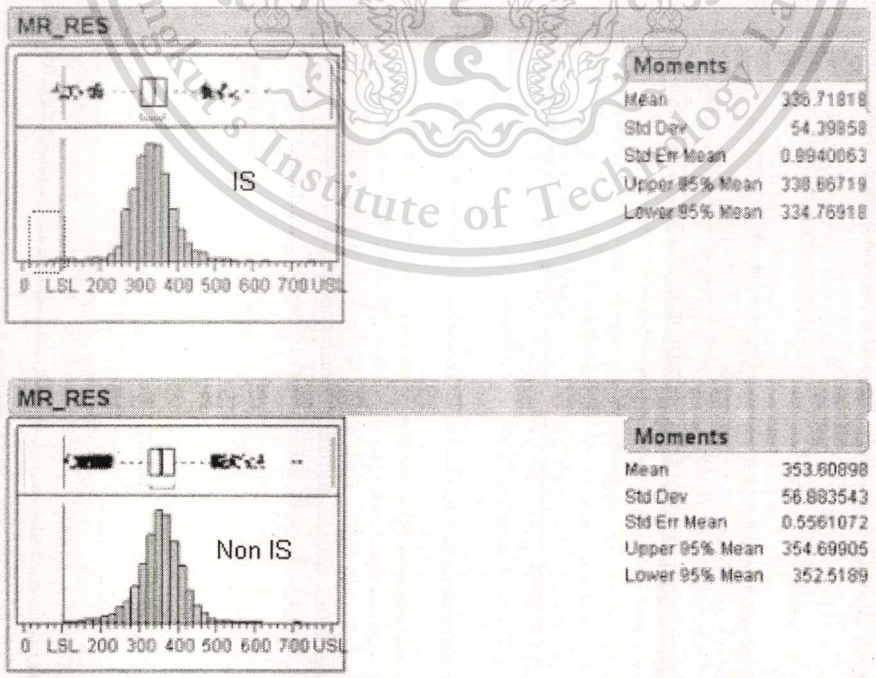

Figure 5.3 Reader resistance distribution of IS and Non IS

Fig. 5.3 compares the MR reader resistance distribution of IS to of non-IS. Non- IS has a higher MR reader resistance mean than MR reader resistance mean of IS (also higher sigma). Therefore, combining with virtual no inflation of the lower distribution tail results in no ESD failure for MR_RES.

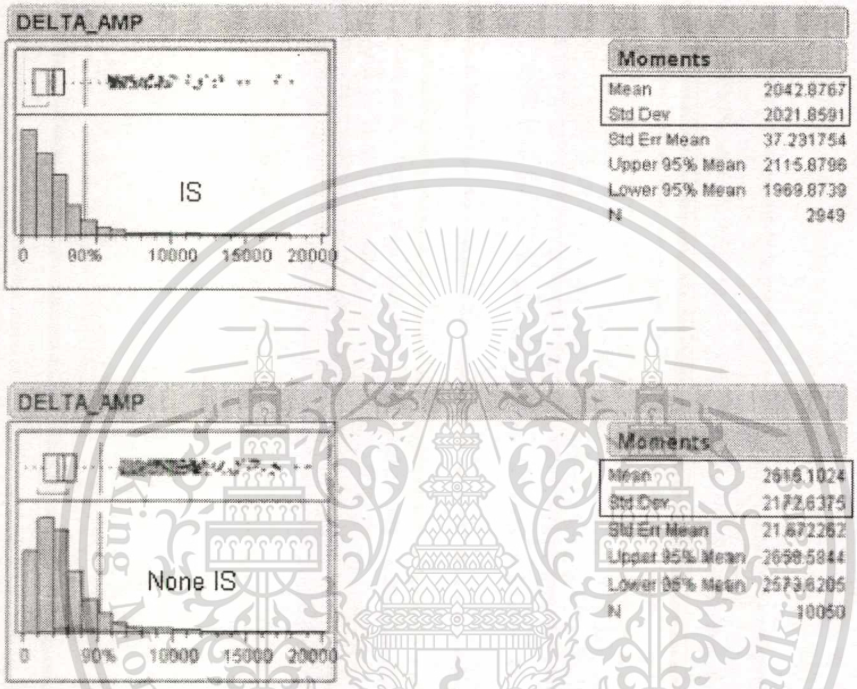

Figure 5.4 Delta Amplitude distribution of IS and Non IS

Fig. 5.4 compares Delta Amplitude distribution of IS to non-IS. Non-IS has significantly higher Delta Amp failure than IS's. Delta amplitude failure corresponds with Amplitude mean and sigma. The highlighted sigma values are in the distribution charts. This is a one-sided distribution. An inflated distribution tail in this case causes the higher sigma for non-IS. The result of non-IS has significantly higher Delta Amp failure than IS's. Therefore, It is quick-checked results. Evaluations are continuing with reliability test.

5.2 IS vs non IS HGA with Vermit reliability test

Second evaluation is 400 Hrs reliability test by Vermit reliability tester. The test concept is in Fig, 5.5. Time To Failure (Life) vs Stress is plotted by specifying the Life-

Stress model using reliability analysis software. The sample 128 sample HGAs / group of IS and Non IS head. The robustness of recording head is then verified using life test. The life tests with multiple stress levels sets varied from low to high voltage are applied to recording heads with long period. The readers are intentionally damaged until resistance changed to target value. Life data is statistical. Life distributions data is analysed by ALTA 6Pro. Fig. 5.5 described the graph details (theory). X-axis is Vzap-type step up from USE level to STRESS level (voltage) until resistance changed to target value. Intentionally damaged readers plotted by Y-axis with, then tested life vs voltage stress for Verifying if a population's median is equal to a target value. With the rule's Wilcoxon Signed- Rank test have apply to this analysis. Graph is non-Parametric Statistics. It is distribution-free statistics. It is branch of statistics that deal with non-normally distributed data.

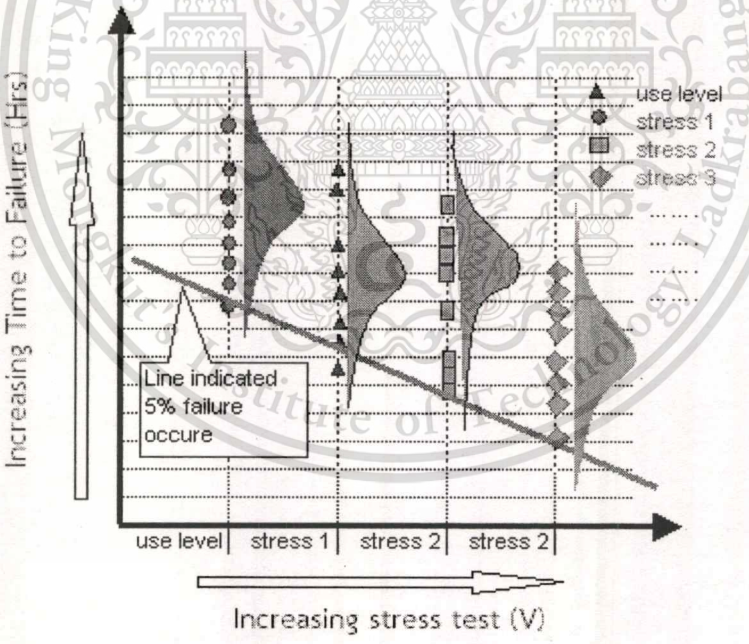

Figure 5.5 Time to failure (TTF) vs Stress is plotted by Life-Stress model

The steps of stress test are sequence as below from sample HGAs IS vs non IS

1. Vermit test procedure

1.1. Life Test Temp and Tool: 85°C in Vermit 4 [Seagate]

1.2. Test Time: ~400 – 660 hours Thailand

1.3. Stress levels: Vary from 0.2~0.35V, 8 step

1.4. Life Analysis: ALTA PRO,

1.5. Failure Criteria: 30% MR change.

2. Complete data set fitted to a given distribution

3. Modeling, use level distribution extrapolated

Fig. 5.6 Graph described the results for evaluation. The stress level is varied from 0.2 to 0.36V. The multiple stress steps by 0.02V per level. MR_ resistance change is used as the indicator of head response. The point of data indicated the failure occurred. The red cycle plot is IS and blue triangle is non IS. The simplify response curve is red and blue line indicated non IS slightly better for short test time (Y-axis) where is prediction 2.5% failure at 7,000 hrs the stress voltage is 0.133 Volt both groups. The interpretation is long life performance of IS and non-IS reader comparable.

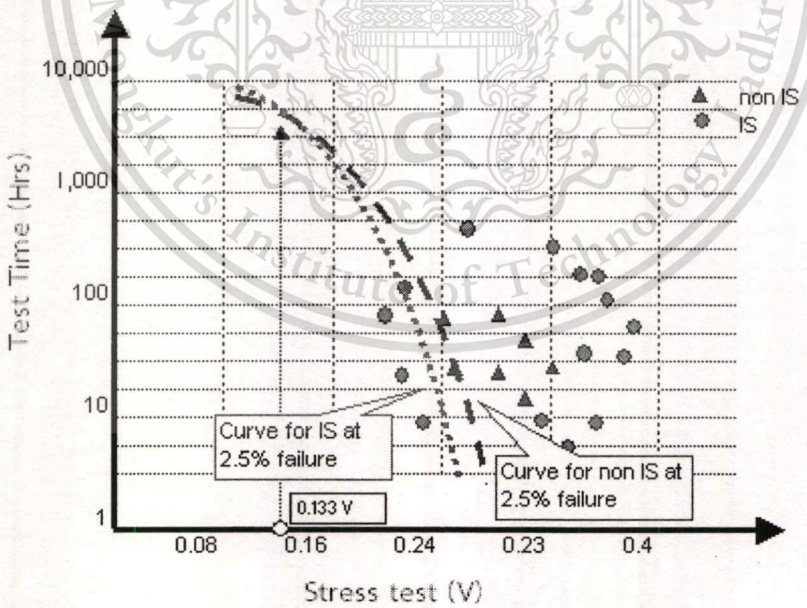

Figure 5.6 Reader life performance with detection of 2.5% failure

The acceleration of failure to quantify product life characteristics with life tests is set at temperature 80-90°C and period of test time 500-600 Hrs.

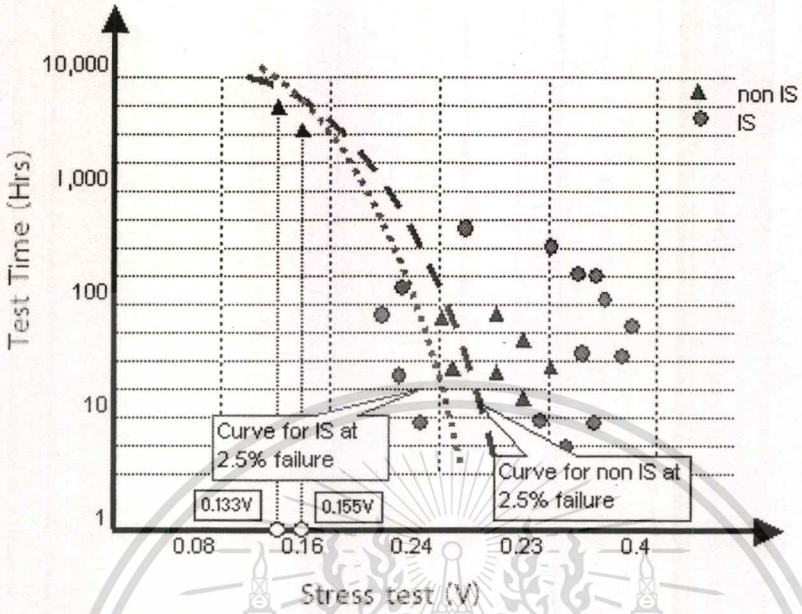

Figure 5.7 Reader life performance with detection of 5% failure

To extend 2.5% to 5.0% failures from same data set. Fig. 5.7, it shows life performance of IS and non-IS are comparable projection around 0.155V at 7,000 hrs.

5.3 Blown shunting evaluation at difference time on IS head

3rd evaluation is blown time shunting at difference time are evaluated (short 1msec., medium 10msec. and long time 100msec.) on IS head. There are 128 HGA samples per/group. The tester heater-controller circuits are programmed to apply a voltage pulse. The tester heater-controller circuits are programmed to apply a voltage pulse vary of 3.5V/100msec., 3.5V/10msec. and 3.5V/1msec. to the heater; the preamplifier diodes sink the fuse current. The opened fuse-link ends are separated by melted alumina.

5.3.1 Compare read back IS of each blow time difference (short, medium and long time) on ETS tester

There are 128 HGA samples per/group. Evaluation set blow time duration by vary at " Short, Medium and Long " blow time with fix voltage. Three level of duration time for blow shut circuit was design for this experiment.

Blow time duration	CUM yield	Related failure	Non related failure	Defect for related failure acceptance interval	Results
1 msec. (short)	43%	2%	55%	1-3%	acceptable
10 msec. (medium)	54%	1.50%	44.50%	1-3%	acceptable
100 msec. (long)	48%	2.20%	49.80%	1-3%	acceptable

Table 5.2 Comparison of IS HGA yield with difference blow time

CUM Yield results does not correlate with blow time. The table 5.2 shows yield (short) is 43%, yield (medium) is 54%, and yield is 48% with blow time at long condition. There are non-related failures confounding. The related failure rang is 1.5-2.2%. Cumulative (Cum) yield is simultaneously fails for multiple ET specs; the failure is follow as hierarchical test. It is importance to verify by individual paramedics test. Related failures are including MR_resistance, Amplitude. Non related failures are BIT ERROR RATE (BER), Areal density Capability (ADC) Head media spacing (HMS) and etc.

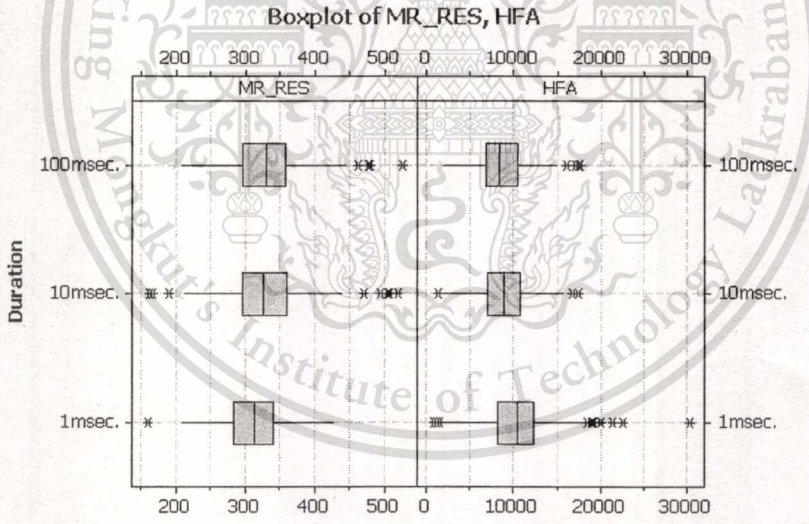

Descriptive Statistics: MR_RES, HFA

Variable	Duration	Mean	SE Mean	StDev	Minimum	Median	Maximum
MR_RES	100msec.	330.41	3.48	49.93	207.29	329.05	525.56
	10msec.	326.24	3.74	53.75	160.77	324.68	520.59
	1msec.	309.88	3.27	46.40	159.03	312.30	424.67
HFA	100msec.	8683	189	2714	1931	8314	17657
	10msec.	8930	204	2928	1119	8774	17480
	1msec.	10484	275	3887	732	10284	30322

Figure 5.8 Read back signal with ETS tester a.) MR_resistance b.) HFA

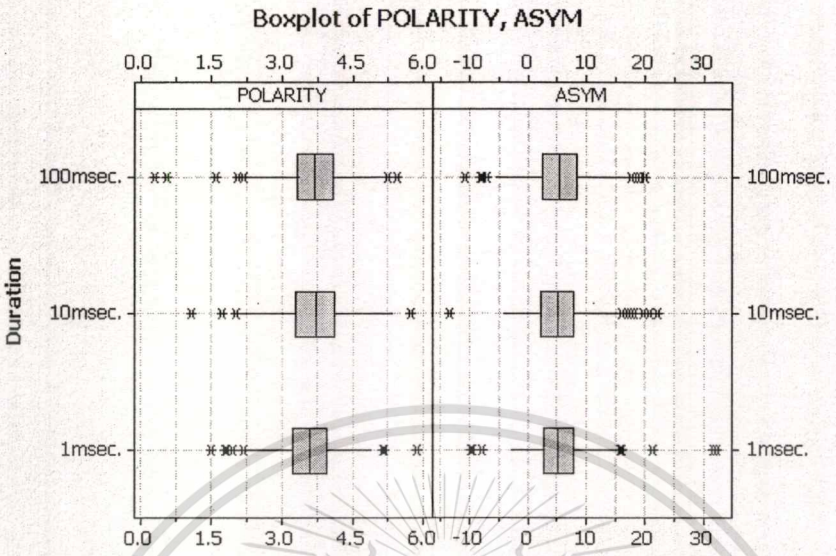

Descriptive Statistics: POLARITY, ASYM

Variable	Duration	Mean	SE Mean	StDev	Minimum	Median	Maximum
POLARITY	100msec.	3.6657	0.0499	0.7168	0.2749	3.6874	5.4295
	10msec.	3.7063	0.0461	0.6615	1.0610	3.7382	5.7305
	1msec.	3.5811	0.0440	0.6223	1.4832	3.5835	5.8558
ASYM	100msec.	5.287	0.355	5.098	-10.998	5.236	19.982
	10msec.	5.206	0.348	5.000	-13.567	4.934	22.061
	1msec.	5.453	0.372	5.259	-9.778	5.117	32.154

Figure 5.9 Read back signal with ETS tester a.) Polarity b.) Asymmetry

Fig 5.8 and Fig 5.9 show the read back signal of key critical parameter MR_RES, High frequency amplitude (HFA), Polarity (POL) and Asymmetry (Asym). The results show that their performances are comparable. Traditional BIT Error Rate (BER) is excluding from this evaluation. Amplitude is writing single-frequency patterns and averaging the peak-to-peak amplitude of the read-back waveform around the track characterize the amplitude of a recording system. These measurements are referred to as TAA, or "Track-Averaged Amplitude. Asymmetry measures the ratio of the positive and negative amplitude pulses. It is a side-product of amplitude tests. Asymmetry is determined by measuring the positive and negative amplitudes in perpendicular recording, it can come from both read and write. Polarity is write pattern and

measure positive and negative peaks. Positive peak values per clock cycle should be larger than negative peak values then write inverted pattern and measure positive and negative peaks. The correct polarity is > 1.

5.3.2 Compare 400 Hours reliability test of each blow time difference (Short, Medium and long time) on Vermit the samples are 128 HGA samples per/group. There are 8 steps

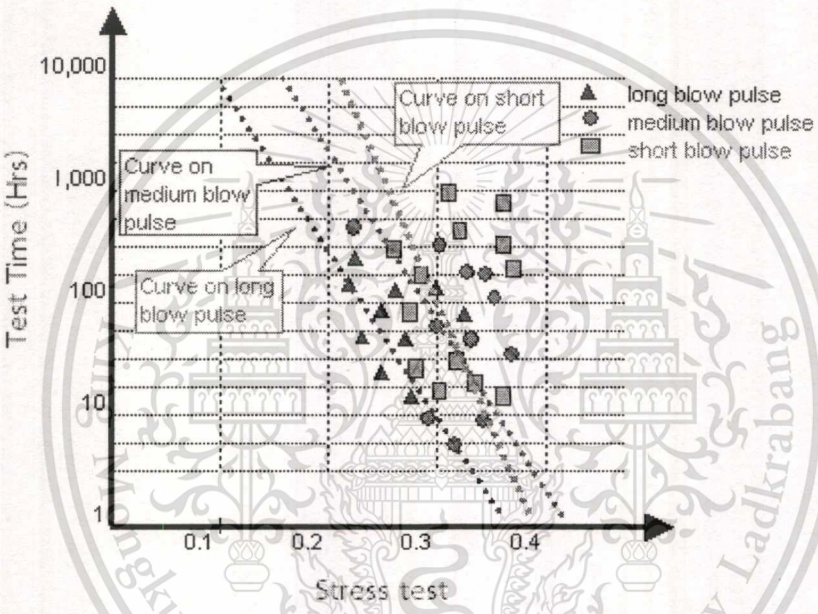

Figure 5.10 Reader life performance comparison 7000 Hrs with blow shunting at difference time (short, medium and long time)

Three groups HGAs set blow time pulse duration apply to HGA by vary at " Short, Medium and Long " with fix voltage. The multiple stress levels set with failure criteria are based on MR- reader resistance threshold. The long blow time (G1T1) to IS get worst for all range of stress level compare to other Medium time (G2T1) and short time (G3T1) blow. The case of medium and short blow, before reaching 1 hrs, the stress levels of medium are higher than that of short blow time, while after 1 hrs, the stress levels of short blow are higher.

5.4 Conclusions

To extend test capability for pad size below tester tolerance limit for 4-pt probing to 2-pt probing, the research has evaluated. Eliminate the significant IS scaling errors in measurements; improve SNR and noise screening capability The quick check results from the study of failure of IS and non IS while processing through production show no significant difference from the samples of recording heads that being tested. The parameter failure is follow as hierarchy test sequence. The ETs setting between IS and non-IS are limit as ability of tester. It was set with difference hierarchy. The parameter distributions were compared by mean and sigma. Consider CUM yield is compared for both groups performance. Its HD performance is same results from quick check. The robustness of recording head is then verified using life test. At 7,000 Hrs with multiple stress levels sets varied from low to high voltage to recording head. A minimum resistance protects against parts which IS are slightly weak, whereas non-IS slightly better at low TTF level while high TTF are the lift is similar both groups of 2.5% to 5% failure. The interpretation is long life performance of IS and non-IS reader comparable. Hypothesis was IS removal may cause damage to the reader barrier. An opportunity to determine if parts with IS are blown with difference blow time of voltage apply to IS show difference. Process for shunt removal at testing to recording head is at HGA ETs before the head is tested on the disc, the tester heater-controller circuits are programmed to apply a voltage pulse of 3.5V/100 msec. to the heater; The long blow time of voltage apply to IS get worst for all range of stress level compare to medium and short blow time of voltage apply to IS. The medium vs short blow time of voltage apply to IS before reaching 1 hrs, the stress levels of medium blow time of voltage apply to IS are higher than short blow time of voltage apply to IS, while after 1 hrs, the stress levels of short blow are higher. The interpretation of this research shown the long blow pulse is too weak to survive warranty periods due to resistance loss.

5.5 Recommendation/ Comment

The research is using the current ETs tester (quick test) and Barrier degradation test is using Vermit life test system to see the reader long-term test at 400-7,000 hrs. Resistance/ Amplitude change vs time and voltage is indicator. ESD control actions have been identified for both Slider and HGA factories time to time. To understand of head physical are determine as.

1.) Stability test (Failure Mechanism: IS removal may cause damage to the reader magnetic which becomes apparent over time/repeated measurements). Their test is required metric of resistance and amplitude. The change vs time and temperature.

2.) Magnetic Performance Test Method (Failure Mechanism: IS removal may cause damage to the reader magnetic). Their test requires metrics of resistance and amplitude vs temperature.

Appendix - A

Failure Mode Testing and Analyses

A.1 Time-dependent dielectric breakdown (TDDB) of magnetic tunnel junction devices [42]

The dielectric breakdown characteristics of magnetic tunnel junctions are the primary reliability concern. It has been found that the distribution of time dependent dielectric breakdown (TDDB), t_{BD}, as a function of stress voltage across a MTJ, VMTJ, closely follows the Weibull distribution

$$F(x) = 1 - \exp\left(-(x/\alpha)^{\beta}\right).$$

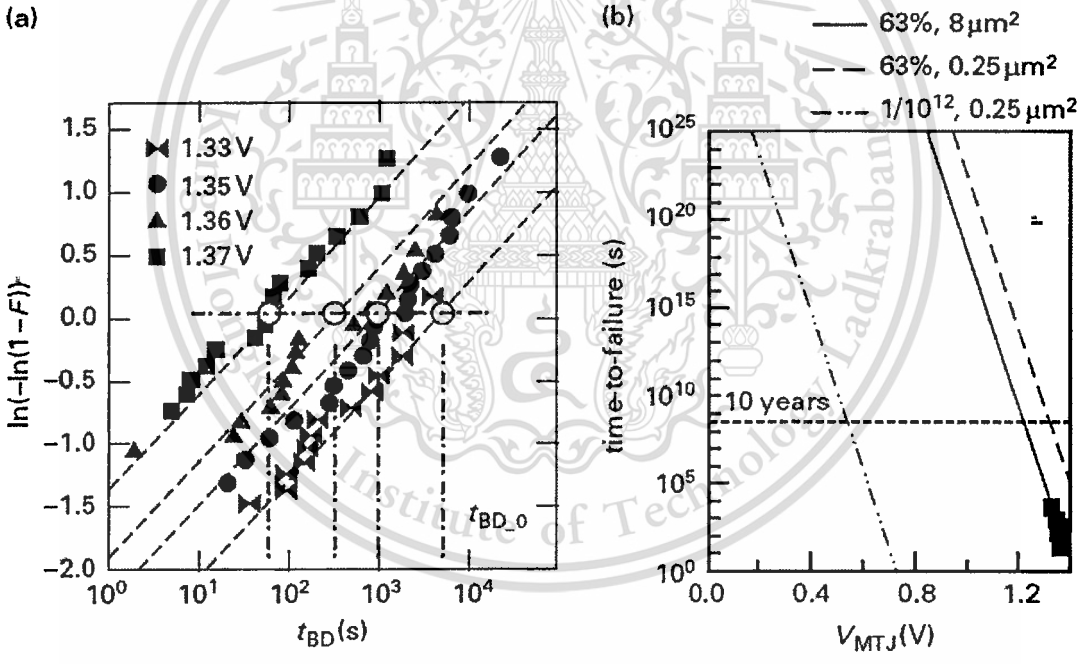

Figure A.1. (a) Weibull plot of time-dependent dielectric breakdown (TDDB) of four different stress voltages; t_{BD_0} is the time at which 63% of the MTJs break down. (b) Time-to-failure vs. VMTJ.

In this case, x is the time-to-breakdown, t_{BD}, at a given stress voltage; α is the scaling factor between t_{BD} and the stress voltage, VMTJ, and β is the activation energy – both are extracted from the Weibull plot. The operating life of a MTJ at a given V_{MTJ} can therefore be projected by

constructing a series of Weibull plots of the TDDB of different V_{MTJ} stress voltages, usually greater than the operating voltage. Thus, the tunnel barrier of the MTJ breaks down in a short time. By measuring the t_{BD} of a large number of MTJs at a stress voltage VMTJ, one obtains the cumulative distribution of $F(t_{BD})$. From $F(t_{BD})$, one may construct one line on the Weibull plot g (t_{BD})ln(-ln(1-$F(t_{BD})$). Repeating the same measurement at a different stress voltage, one can construct another line. Figure A.1(a) shows the Weibull plots of $g(t_{BD})$ of four stress voltages. The slope of $g(t_{BD})$ the data line of each stress voltage is roughly the same. For each stress voltage V_{MTJ}, 63% of the devices break down at a time that each curve intersects at $g(t_{BD\_0}) = 0$. Knowing β, one can project the operating voltage of the MTJ at a breakdown probability of 10^{-12}.

A.2 Defect density and the breakdown/TMR distribution of MTJ devices

The probability of n events, given a mean rate of λ is

$$P(n, \lambda) = (\lambda^n / n!) \exp(-\lambda).$$

The average number of defects (the "rate," as above) $\lambda = d * A$, where d is the defect density (number of defects/mm2) and A is the MTJ area. The probability that a bit cell with area A has zero defects is

$$P(n = 0 , d * A) = \exp(-d * A).$$

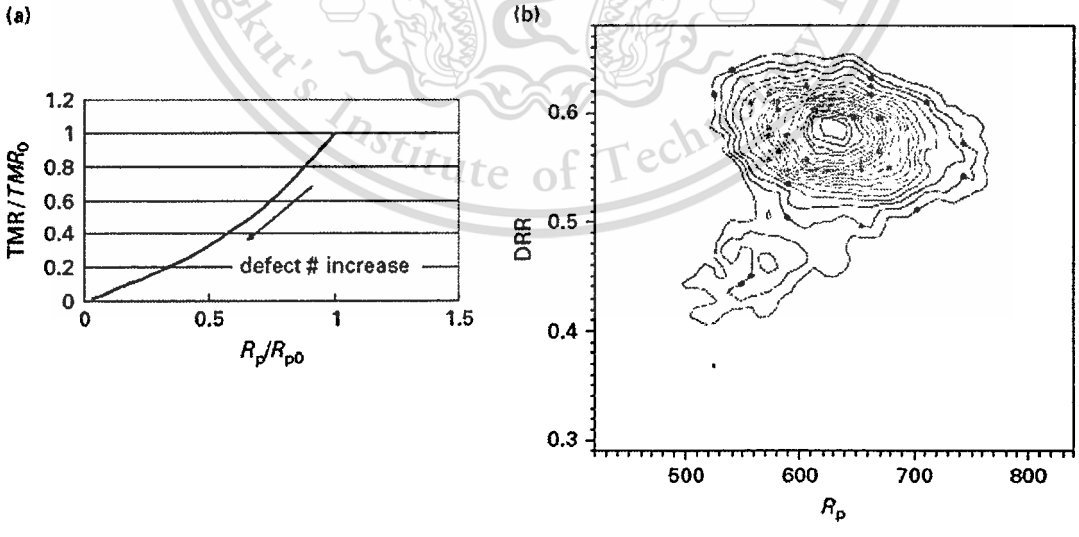

Figure A.2. (a) TMR vs. R_p affected by defects from this model. (b) Measured distribution of TMR vs. R_p. (Courtesy of Robert Beach, MagIC Technologies, Inc.)

We postulate that bit cells with no defects exhibit hard (intrinsic) breakdown and bit cells with defects exhibit soft (extrinsic) breakdown. The population of soft breakdown increases as the defect number increases.

Similarly, a defect in a MTJ is considered as a finite resistance, which does not contribute to the TMR action. So, a MTJ with n defects may be modeled as a MTJ in shunt with n fixed resistances:

$$1/R_L = 1/R_p + n\ /R_{defect}$$

Thus, if $x = n * (R_p/R_{defect}) << 1$, then $R_L \approx R_p(1-x)$ Similarly, based on the same argument, it follows that

$$TMR = R_H / R_L - 1 \approx TMR_0[1-(x+x') * (TMR_0 + 1)],$$

where $x' = n * R_{ap} / R_{defect}$. Both R_p and the TMR drop off when the number of defects increases. Figure A.2 illustrates the effects of measured TMR vs. R_p.

A.3 Acronyms, Definitions and Symbols

This thesis document uses the following set of Acronyms, definitions and Symbols

IS	Internal Shunting
GMR	Giant Magneto Resistive
TGMR	Tunneling Giant Magneto Resistive
SPH	Single Pole Head
ESD	Electro Static Discharge
TDDB	Time- Dependent Dielectric Breakdown
ABS	Air bearing Surface
STE	Side- Track Erasure
ATI	Adjacent Track Interference
MIR	Multiple Image Reflection
MFM	Magnetic Force Microscopy
BEM	Boundary Element Modeling
SSPH	Shield Single Pole Head
SUL	Soft Under Layer
RL	Reference Layer
FL	Free Layer
HBM	Human Body Model
MM	Machine Model
CDM	Charged Device Model
RF	Radio Frequency

REFERENCE

[1] Anthony, "Effect of GMR Recording Head Resistance on Human Body and Machine Model ESD Waveforms, "1-58537-040-1/2002/$10.00 ©2002 ESDA, pp. 340

[2] A.Siritaratiwat, N.Suwannata, J Pinnoi and C Puprichitkun, " ESD Effect in GMR heads in the Trim Shunt Tab process," *IEEE 8th IPEA*, pp.126-129, 2001.

[3] Al Wallash., "ESD SPICE Model and Measurements for a Hard Disk Drive, "Maxtor Corporation, 500 McCarthy Blvd, Milpitas, CA 95035.

[4] A. Wai Yuen, E. Cheuk Leung, P. Kin Wong, T Shimizu, T. Kagami, M. Dovek and David Hu, " Anti-static robustness enhancement and high – frequency noise pickup immunity by internal shunting for tunneling magnetoresistive sensors. *IEEE,* vol. 44,pp. 104-106, Jan., 2008.

[5] A.Wallas et al., " ESD evaluation of tunning magnetoresisitive (TuMR) device, " *in ESD/EOS Symp. Proc.,* 2000, p. 470.

[6] L. Baril, " Degradation of GMR and TMR recording heads using very- short-duration ESD transients, " *IEEE Trans. Magn.*, vol. 38, no.5, P.2283, Sep. 2002.

[7] Z.Y. Teng et al., " Breakdown behavior of TMR head in ESD transients," *in EOS/ESD Symp. Proc.,* 2004, p.346.

[8] A. S. Hoagland, "History of magnetic disk storage based on perpendicular magnetic recording," *IEEE Trans. Magn.* 39 (4), 1871 (2003).

[9] F. Liu, K. Stoev, P. Luo, Y. Liu, Y. Chen, J. Chen, J. Wang, S.F.Gu, K.T. Kung, M. Lederman, M. Krounbi, M. Re, A. Otsuki, S. Hong, "Perpendicular recording heads for extremely high-density recording," *IEEE Trans. Magn.* 39 (4), 1942 (2003).

[10] Private Communications with Mark Kryder, CTO of Seagate Technology (2003).

[11] S. Iwasaki and Y. Nakamura, "An analysis for the magnetization mode for high density magnetic recording, "*IEEE Trans. Magn.* 13, 1272 (1977).

[12] W. P. Jayasekara, S. Khizroev, M. H. Kryder, W. Weresin, P. Kasiraj, Fleming, "Inductive write heads using high moment FeAlN pole," *IEEE Trans. Magn.* , 35 (2) pt.1, 613-8 (1999).

[13] S. Khizroev, A. Lyberatos, M. H. Kryder, and D. Litvinov, "Physics of perpendicular recording: effects of magnetic "charge" distribution," *Japanese J. Appl. Phys., Part 2 Letters* 41 (7A), L758-60 (2002).

[14] S. Iwasaki and Y. Nakamura, "An analysis for the magnetization mode for high density magnetic recording, "*IEEE Trans. Magn.* 13, 1272 (1977).

[15] George J. Y. Fan, "Analysis of a practical perpendicular head for digital purposes," *J. Appl. Phys.* 31(5), 402S (1960).

[16] H. Takano, Y. Nishida, T. Hamaguchi, F. Tomiyama, Y. Kawato, H. Sawaguchi, F. Tomiyama, Y. Kawato, H. Sawaguchi, H. Aoi, N. Ohta, "A practical approach for realizing high-recording-density HDDs by using perpendicular recording," presented at the AIT-MINT 2001 Workshop on Magnetic Information Storage Technology, March, 2001.

[17] F. Liu, K. Stoev, L. Leal, J. Wang, Y. Chen, S. Shi, H. Tong, M. Lederman, M. Re, "Perpendicular high areal densities and high data rates," presented at the AIT-MINT 2001 Workshop on Magnetic Information Storage Technology, March, 2001.

[18] S. H. Charap, P.-L. Lu, Y. He "Thermal Stability of Recorded Information at High Densities, "*IEEE Trans. Magn.* 33 (1), 978 (1997).

[19] D. A. Thompson and J. S. Best, "The Extendibility of Magnetic Recording for Data Storage," *IBM Executive Briefing*, January 1998.

[20] W. Cain, A. Payne, M. Baldwinson, R. Hempstead, "Challenges in the practical implementation of perpendicular magnetic recording," *IEEE Trans. Magn.* 32 (1), 97 (1996).

[21] S. Khizroev, J. A. Bain, M. H. Kryder, "Considerations in the design of probe heads for 100 Gbit2 recording density," *IEEE Trans. Magn.*, 33 (5), pt.1, 2893 (1997).

[22] D. Litvinov, M. Kryder, and S. Khizroev, "Recording physics of perpendicular media: soft underlayer," *JMMM* 232 (1-2), 84-90 (2001).

[23] D. Litvinov, M. Kryder, S. Khizroev, "Recording physics of perpendicular media: recording layer," *JMMM* 232, 84 (2001).

[24] S. Khizroev, Y. Liu, K. Mountfield, M. Kryder, D. Litvinov, "Physics of perpendicular magnetic recording: writing process," *JMMM* 246 (1-2), 335-44 (2002).

[25] S. Khizroev, M. H. Kryder, Y. Ikeda, K. Rubin, P. Arnett, M. Best, D. A. Thompson, "Recording heads with trackwidths suitable for 100 Gbit/in2 density, " presented at Intermag'99, May 1999, *IEEE Trans. Magn.* 35 (5), 2544 (1999).

[26] S. Khizroev, M. Kryder, and D. Litvinov, "Next generation perpendicular systems," *IEEE Trans. Magn.* 37 (4), 1922 (2001).

[27] R.P. Hunt, "A magneto-resistive readout transducer," *IEEE Trans. Magn.* 7, 1 (1971).

[28] D.A. Thompson, "Magnetoresistive transducers in high-density magnetic recording," *AIP Conf. Proc.* 24, 528 (1975).

[29] D.A. Thompson, L.T. Romankiw, A.F. Mayadas, "Thin film magnetoresistors in memory storage and related applications," *IEEE Trans. Magn.* 11 (4), 1039-50 (1975).

[30] R.S. Indeck, J.H. Judy, and S. Iwasaki, "A magnetoresistive Gradiometer," *IEEE Trans. Magn.* 24 (6), 2617 (1988).

[31] H.S. Gill, V.W. Hesterman, G.J. Tarnopolsky, L.T. Tran, P.D. Frank, H. Hamilton, "A magnetoresistive gradiometer for detection of perpendicularly recording magnetic transitions," *J. Appl. Phys.* 65 (1), 402 (1989).

[32] D.J. Mapps, "An inter-digitated magnetoresistive reply head," U.K. Patent 2,143,071, October 28, 1987.

[33] R.E. Jones, Jr., M.H. Kryder, K.R. Mountield, J.I. Guzman, "Unshielded horizontal magnetoresistive head and method of fabricating same," US Patent 5,155,643, October 13, 1992.

[34] J.C. Mallinson, "Gradiometer Head Pulse Shapes," *IEEE Trans. Magn.* 26 (2), 1123 (1990).

[35] G.J. Fan, "A study of the playback process of a magnetic ring head," *IBM J. of Res. & Dev.* 5, 321-325 (1961).

[36] N. Smith, D. Wachenshwantz, "Magnetoresistive heads and the reciprocity principle," *IEEE Trans. Magn.* 23 (5), 2494 (1987).

[37] S. Khizroev, J. A. Bain, M. H. Kryder, "Considerations in the design of probe heads for 100 Gbit2 recording density," *IEEE Trans. Magn.* 33 (5), pt.1, 2893-5 (1997).

[38] M. Mallary, A. Torabi, M. Benakli, "1 Tb/in2 Perpendicular Recording Conceptual Design," *IEEE Trans. Magn.* 38, 1719 (2002).

[39] M. Mallary, A. Torabi, M. Benakli, "1 Tb/in2 Perpendicular Recording Conceptual Design," *IEEE Trans. Magn.* 38, 1719 (2002).

[40] R.E. Fontana, B. Gurney, T. Lin, V. Speriosu, C. Tsang, D. Wilhoit, U.S. patent #5,701,223.

[41] K. Suzuki et al. IEEE Transactions on Electron Devices, 1996; ED-43(7): 1166.

[42] J. Das, R. Degraeve, P. Roussel, G. Groeseneken, G. Borghs and J. De Boeck, J. Appl. Phys. 91(10), 7712 (2002).

[43] Scofield " Four-Probe Resistance Primer ", Physics 414. 2000.

[44] QST-2002 External test, Integral solution INT'L. SAN JOSE, 2002

[45] S. Voldman. ESD : *Physics and Devices. Chichester, England*: Jonh Wiley and Sons, 2004.

[46] S. Voldman. ESD : *Circuit and Devices. Chichester, England*: Jonh Wiley and Sons, 2006.

[47] A Wai Yeun Lai and A Wallash, " Effect of GMR recording head resistance on human body and machaine model ESD waveforms," *IEEE ESDA*, pp. 340-344, 2002.

[48] S. Khizroen and D Litvinov, " Perpendicular magnetic recording," Springer science, 2005.

[49] Jeffrey R. Childress and Robert E. Fontana Jr. " Magnetic recording read head sensor technology ", C. R. Physique 6 (2005) 997–1012.

JICTEE 2010

Programs and Abstracts

Joint International Conference on Information & Communication Technology, Electronic and Electrical Engineering
JICTEE 2010

LuangPrabang, Lao PDR. 21-24 December, 2010

Effects of Internal Shunting (IS) to Recording Head

Jiropast Suakaew[1], Wanchai Pijitrojana[2], Kasin Vichienchom[3]

[1]*College of Data Storage Technology and Applications, King Mongkut's Institute of Technology Ladkrabang, Thailand.*

[2] *Faculty of Engineering, Thammasat University, Klong Luang Pathumthan, Thailand.*

[3]*Faculty of Engineering, King Mongkut's Institute of Technology Ladkrabang, Thailand.*

Abstract— **This research is concerned with the study of effects from Internal Shunting (IS) on recording head. IS has been introduced on tunnelling giant magneto resistive heads to enhance the device anti-static robustness and the external high-frequency noise pickup immunity. The shunting scheme and its mechanism lead to both increasing anti-static robustness and reducing high-frequency noise pickup. The newest TGMR products, however, there are multiple pads with smaller in pad sizing and complicated in structure. The TGMR test pad is smaller than the measurement probe, the current standard probing 4pt probing is required to maintain measurement accuracy with IS scaling error minimized, It is accuracy measurement than 2pt Tip. Therefore, 4pt probing is limited to measure high areal density recording head at point of use from error scaled. To solve this manufacturing complication, the non – IS design now being considered for new coming recording head as of 2pt probing accuracy is acceptable. To analyse the effects of IS vs non-IS, the readout signal amplitude and the head resistance are used as the key parameters to measure the outcome by comparing the head performance of IS and non-IS at the beginning of the assembly process with that at the ending of the assembly process. The study results show failure of IS and non-IS while processing through production are not significantly different from sample recording head that being tested. The robustness of recording head is then verified using life test. The 7,000 Hrs life tests with multiple stress levels sets varied from low to high voltage are applied to recording heads. The readers are intentionally damaged until resistance changed to target value. There is no sign of difference of resistance and amplitude changed with time and voltage from two groups of samples, IS and non-IS.**

Keywords— **Internal Shunting, HBM, MM, CDM, IS**

I. Introduction

The use of an ultra-thin insulating barrier and the presence of conductive paths in the form of pinholes are the key concerning for the performance of the tunnelling giant magneto resistive (TGMR) sensor to be indeed easily degraded by ESD [1-4]. To handle this matter, the internal shunting (IS) has been introduced on (TGMR) head [5]. It is able to enhance anti-static robustness and external high-frequency noise pickup immunity of the device. Details of simplified schematic diagram of the recording head with and without shunting are shown in Fig. 1(a) and (b).

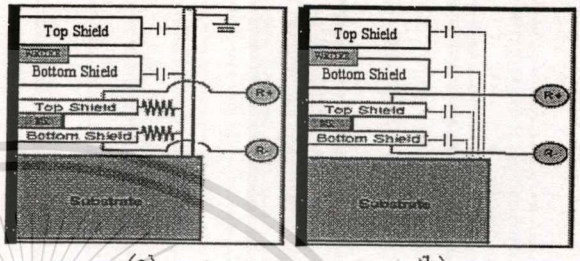

Fig. 1. Schematic diagram of recording head (a) IS and (b) Non-IS

For the recording head with IS as shown in Fig.1 (a) If capacitance between writer bottom shield-to-top MR shield and substrate-to-bottom MR shield are balance, noise injection on both top and bottom shields will be the same for both amplitude and phase. Therefore, noise will be cancelled out for the differential read back signal. In case of non-IS as shown in Fig.1 (b), if noise frequency is high enough, noise current from the substrate can be injected into TGMR sensor due to unbalanced coupling to the top and bottom shields. Since the top and bottom shields constitute the two leads of the TGMR device, this high-frequency noise signal will affect the spectral signal-to-noise ratio measurement.

Due to its scaling error for MR resistance measurement, multi-4pt probing [6] is required for ISI [7] slider test to maintain test accuracy. Fig.2 shows sliders with multiple pads, (a) for low areal density (AD) media and (b) for high areal density media. Comparing both the sliders, the pad size of the high areal density slider is 40% smaller than that of low areal density slider. Because of its smaller pad size, measurement with 4pt probing technique on the high areal density slider can result in large amount of error.

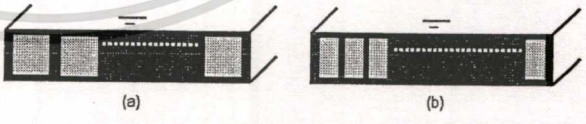

Fig. 2. Slider with multiple probing pad (a) for low areal density media (b) for high areal density media

Sizes of probe tips used in 4pt probing and pads of the low areal density slider and the high areal density slider are illustrated in Fig.3.

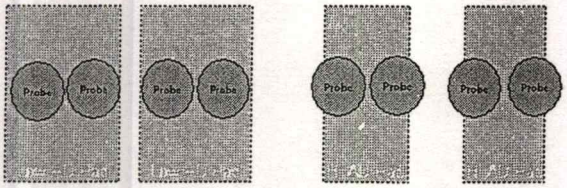

(a) 4pt with low AD pad (b) 4pt with Hi AD pad

Fig. 3. Probe 4pt Tip to slider pad comparison of low areal and high areal density slider.

Since the non-IS design requires only 2pt probing, therefore, each pad needs to accommodate only one probe tip. As a result, the non-IS design is suitable for the smaller pad size of the high areal density slider as shown in Fig.4. Consequently, this design is being considered for new coming recording head.

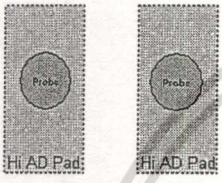

Fig. 4. Probe 2pt Tip to slider pad of high areal density slider.

TGMR sensors are used in magnetic recording as read transducers and it is well known that they are highly susceptible to damage from ESD. It is therefore highly valuable to characterize the ESD damage thresholds and failure mechanisms of these devices by doing human body model (HBM), machine model (MM) and direct charged device model (DCDM) testing [9][10].

This study is carried out on high risk ESD items at the process [11] while being produced the HGA, included of any automated or manual operations in HGA process which involve direct contact to MR element, such as HGA assembly process and testing process.

II. Product Robustness Results

To evaluate the product robustness, head resistance (R) and readout signal amplitude (Amp) of IS and non-IS designs are measured at the beginning and at the end of the assembly process. Two additional metrics are defined as follows. Delta R is the difference of the measured head resistance before and after the assembly process. Similarly, delta Amp is the difference of the measured readout signal amplitude before and after the assembly process. These metrics are used to determine the percent failure of the design due to ESD according to the target specification as shown in table 1.

TABLE I
Comparisons Non IS vs IS performance

Metrics	Conditions for Failure	Percent of Failure	
		Non-IS	IS
Delta R	>10%	2.16 %	6.63%
R	< Min. or > Max.	0%	0.21%
Delta Amp	Min. delta	6.08%	0.89%
Cum		8.24%	7.73%

Table 1 shows cumulative percent failure (Cum). The IS has lower Cum (percent of failure) than non-IS, 7.73% vs. 8.24%, but it is not show a significant difference. Non-IS has lower delta resistance failure while has higher amplitude failure than IS does.

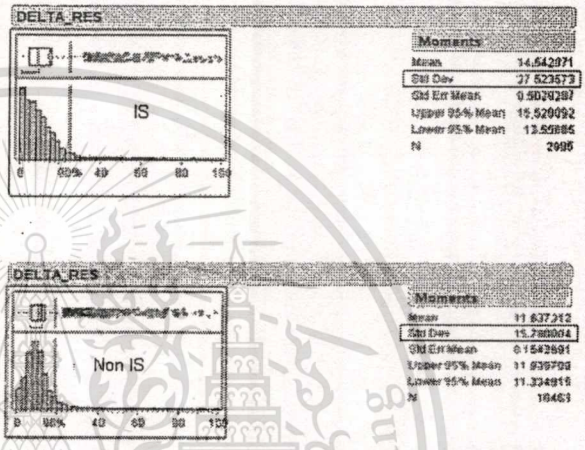

Fig. 5. Delta reader resistance distribution of IS and Non IS

Fig. 5 compares the delta reader resistance of IS to Non-IS. Lower delta resistance failure corresponds with lower delta resistance sigma. The highlighted sigma values are in the distribution charts. This is a one-sided distribution. An inflated distribution tail in this case causes the higher sigma for IS.

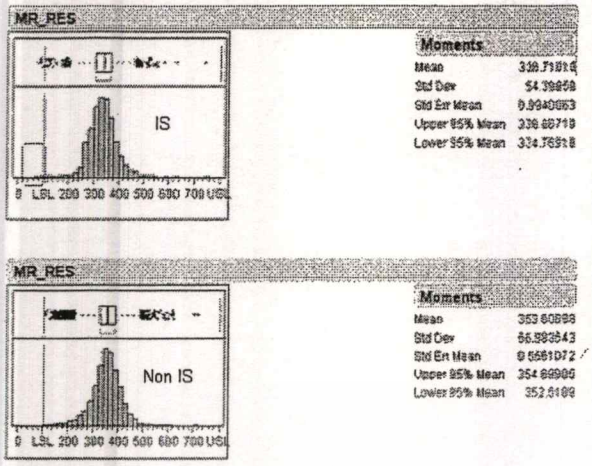

Fig. 6. Reader resistance distribution of IS and Non IS.

Fig. 6 compares the MR reader resistance distribution of IS to of non-IS. Non- IS has a higher MR reader resistance mean than MR reader resistance mean of IS (but also higher sigma). Therefore, combining with virtual no inflation of the lower distribution tail results in no ESD failure for MR_RES.

Fig. 7 compares Delta Amplitude distribution of IS to of non-IS. non-IS has significantly higher Delta Amp failure than IS's. Lower delta amplitude failure corresponds with lower delta amplitude mean and sigma. The highlighted sigma values are in the distribution charts. This is a one-sided distribution. An inflated distribution tail in this case causes the higher sigma for non-IS. The result of non-IS has significantly higher Delta Amp failure than IS's.

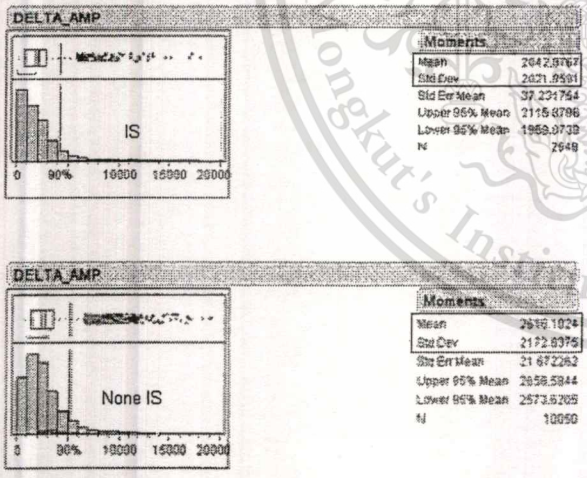

Fig. 7. Delta Amplitude distribution of IS and Non IS.

III. Device Failure Model Test

The Device failure models are applicable for any components of Hard Disc Drive with the basic of RLC. The RLC model for a disk drive [12] was to include enough complexity to make it realistic, but to keep it simple enough so that an intuitive understanding of ESD behaviour could be extracted.

The acceleration of failure to quantify product life characteristics with life tests at temperature 80-90°C and test time 400-600 hrs. The stress level is varied from 0 to 0.4V. The multiple stress levels set with failure criteria are set based on MR- reader resistance threshold.

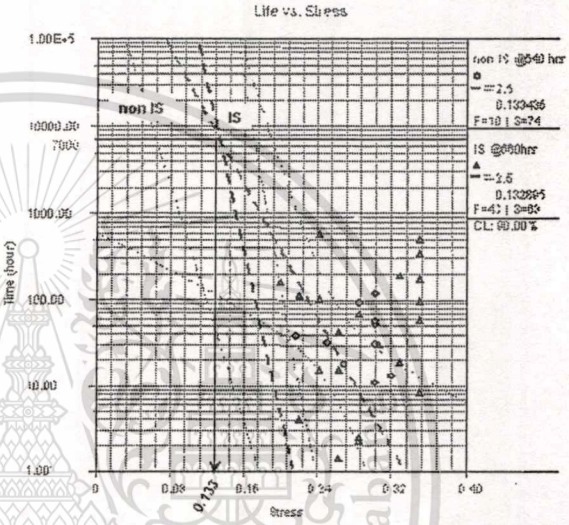

Fig. 8. Reader life performance comparison 7000 Hrs with 2.5% failure.

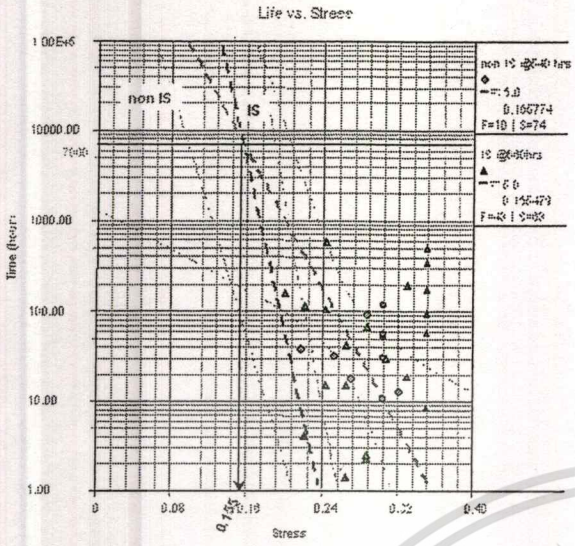

Fig. 9. Reader life performance comparison 7000 Hrs with 5% failure.

Fig. 8 shows life performance comparison of IS and non-IS reader. Both of them show 2.5% failure projection around 0.133 V at 7,000 hrs. To compare with Fig. 9, it shows life performance of IS similar to reader comparing to of non-IS. Furthermore, both of them also show 5% failure projection around 0.155V at 7,000 hrs. In both cases, before reaching 7,000 hrs, the stress levels of non- IS reader are higher than that of IS, while after 7,000 hrs, the stress levels of non-IS are lower than that of IS reader.

IV. Conclusions

The results from the study of failure of IS and non IS while processing through production show no significant difference from the samples of recording heads that being tested. The robustness of recording head is then verified using life test. At 7,000 Hrs with multiple stress levels sets varied from low to high voltage to recording head. The readers are intentionally damaged until resistance changed to target value. There is no sign of difference of resistance and amplitude changed with time and voltage from two groups of samples of IS and non-IS.

V. References

[1] A.Wallas., "ESD evaluation of tunning magnetoresisitive (TuMR) device," *ESD/EOS Symp.*, p. 470, 2000.

[2] L. Baril., "Degradation of GMR and TMR recording heads using very-short-duration ESD transients," *IEEE Trans. Magn.*, vol. 38, P.2283, No.5, Sep. 2002.

[3] Z.Y. Teng et al., "Breakdown behavior of TMR head in ESD transients," in *EOS/ESD Symp. Proc.*, p.346, 2004.

[4] A.Siritaratiwat, N.Suwannata, J Pinnoi and C Puprichitkun., "ESD Effects in GMR heads in the Trim Shunt Tab process," *IEEE 8th IPEA*, pp.126-129, 2001.

[5] A. Wai Yuen, E. Cheuk Leung, P. Kin Wong, T Shimizu, T. Kagami, M. Dovek and David Hu., "Anti-static robustness enhancement and high – frequency noise pickup immunity by internal shunting for tunneling magnetoresistive sensors," *IEEE Trans. Magn.*, vol. 44, pp. 104-106, Jan. 2008.

[6] Scofield., "Four-Probe Resistance Primer," *Physics* 414, 2000.

[7] "QST-2002 External test". *Integral solution INT'L* ., SAN JOSE, 2002.

[8] Y. Zheng, G. Han, K. Li, Z. Guo, J. Qiu, S. Tan,Z. Liu, B. Liu and Y. Wu., "Side – shield TGMR reader with track width reduction scheme," *Intermag*, pp. 348, 2006.

[9] Steven H. Voldman, *"ESD:Physics and Devices"* John Wiley and Sons., England, 2004.

[10] Steven H. Voldman, *"ESD:Circuit and Devices"* John Wiley and Sons., England, 2006.

[11] A Wai Yeun Lai and A Wallash., "Effects of GMR recording head resistance on human body and machine model ESD waveforms," *IEEE ESDA*, pp. 340-344, 2002.

[12] A Wallash., "ESD spice model and measurements for a hard disk drive," *EOS/ESD Symposium*, 2003.

BIOGRAPHY

Name: Mr. Jiropast Suakaew
Date of Birth: April 15, 1969
Place of Birth: Bangkok, Thailand
Educations:

1991 King-Mongkut Institute of Technology Ladkrabang, Faculty of Engineer
1997 Chulalongkorn University, Faculty of Engineer (M.Eng.)

Scholarships:

2009 - 2010 Scholarship for study in the M.Eng. of Data Storage Technology (English program) by NSTDA, KMITL and Seagate Technology (Thailand) Ltd.

Publications:

1. Jiropast S. " Development of a Remote Controlled Robotic Arm for High Activity Source Manipulation", Chulalongkorn University, 1997.
2. Jiropast Suakaew, Wanchai Pijitrojana and Kasin Vichienchom. "Effects of Internal Shunting (IS) to Recording Head", JICTEE, 2011.